

JUN 05 1976



**FEASIBILITY STUDY FOR THE USE OF AN
ELECTROMAGNETIC RAIL GUN IN THE
LAUNCHING AND SUSTAINING OF
REENTRY MODELS**

**VON KÁRMÁN GAS DYNAMICS FACILITY
ARNOLD ENGINEERING DEVELOPMENT CENTER
AIR FORCE SYSTEMS COMMAND
ARNOLD AIR FORCE STATION, TENNESSEE 37389**

April 1976

Final Report for Period May 8, 1974 — September 8, 1975

Approved for public release; distribution unlimited.

Prepared for

**DIRECTORATE OF TECHNOLOGY
ARNOLD ENGINEERING DEVELOPMENT CENTER
AIR FORCE SYSTEMS COMMAND
ARNOLD AIR FORCE STATION, TENNESSEE 37389**

NOTICES

When U. S. Government drawings specifications, or other data are used for any purpose other than a definitely related Government procurement operation, the Government thereby incurs no responsibility nor any obligation whatsoever, and the fact that the Government may have formulated, furnished, or in any way supplied the said drawings, specifications, or other data, is not to be regarded by implication or otherwise, or in any manner licensing the holder or any other person or corporation, or conveying any rights or permission to manufacture, use, or sell any patented invention that may in any way be related thereto.

Qualified users may obtain copies of this report from the Defense Documentation Center.

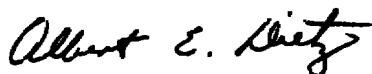
References to named commercial products in this report are not to be considered in any sense as an endorsement of the product by the United States Air Force or the Government.

This report has been reviewed by the Information Office (OI) and is releasable to the National Technical Information Service (NTIS). At NTIS, it will be available to the general public, including foreign nations.

APPROVAL STATEMENT

This technical report has been reviewed and is approved for publication.

FOR THE COMMANDER



ALBERT E. DIETZ
Requirements Planning
Division
Directorate of Technology



ROBERT O. DIETZ
Director of Technology

UNCLASSIFIED

REPORT DOCUMENTATION PAGE		READ INSTRUCTIONS BEFORE COMPLETING FORM
1 REPORT NUMBER AEDC-TR-76-38	2 GOVT ACCESSION NO.	3 RECIPIENT'S CATALOG NUMBER
4. TITLE (and Subtitle) FEASIBILITY STUDY FOR THE USE OF AN ELECTROMAGNETIC RAIL GUN IN THE LAUNCHING AND SUSTAINING OF REENTRY MODELS		5 TYPE OF REPORT & PERIOD COVERED Final Report-May 8, 1974 September 8, 1975
		6 PERFORMING ORG. REPORT NUMBER
7. AUTHOR(s) John P. Barber, Research Institute, University of Dayton, Dayton, Ohio		8. CONTRACT OR GRANT NUMBER(s)
9 PERFORMING ORGANIZATION NAME AND ADDRESS Arnold Engineering Development Center(DY) Air Force Systems Command Arnold Air Force Station, Tennessee 37389		10. PROGRAM ELEMENT, PROJECT, TASK AREA & WORK UNIT NUMBERS Program Element 65802F
11 CONTROLLING OFFICE NAME AND ADDRESS Arnold Engineering Development Center(DYFS) Air Force Systems Command Arnold Air Force Station, Tennessee 37389		12. REPORT DATE April 1976
		13. NUMBER OF PAGES 80
14 MONITORING AGENCY NAME & ADDRESS(if different from Controlling Office)		15. SECURITY CLASS. (of this report) UNCLASSIFIED
		15a. DECLASSIFICATION/DOWNGRADING SCHEDULE N/A
16 DISTRIBUTION STATEMENT (of this Report) Approved for public release; distribution unlimited.		
17 DISTRIBUTION STATEMENT (of the abstract entered in Block 20, if different from Report)		
18. SUPPLEMENTARY NOTES Available in DDC		
19 KEY WORDS (Continue on reverse side if necessary and identify by block number) <div style="display: flex; justify-content: space-between;"> <div> feasibility study electromagnetic rail gun launching </div> <div> sustaining reentry models velocity </div> </div>		
20 ABSTRACT (Continue on reverse side if necessary and identify by block number) <p>The requirements of a realistic reentry test facility for aerothermodynamic tests are reviewed. Basically, this requires the test article to be accelerated to a high velocity and then exposed to the test environment for a sufficient length of time. One method which might be considered to accelerate the test model to the required velocity is an electromagnetic launcher. Equations are developed to describe the performance of several</p>		

UNCLASSIFIED

UNCLASSIFIED

20. ABSTRACT (Continued)

variations of an electromagnetic launcher, as well as component specifications and approximate costs. A similar effort is devoted to the problem of sustaining the velocity by electromagnetically providing a force to overcome the aerodynamic drag and friction forces during testing. Component specifications are developed and costs estimated.

UNCLASSIFIED

PREFACE

The study reported herein was conducted by the Arnold Engineering Development Center (AEDC), Air Force Systems Command (AFSC), under Program Element 65802F. The results were obtained by ARO, Inc. (a subsidiary of Sverdrup & Parcel and Associates, Inc.), contract operator of AEDC, AFSC, Arnold Air Force Station, Tennessee. The work was done under ARO Project Numbers VF419-12GA, V31S-36A, and V31S-02A. The author of this report was John P. Barber, Consultant to ARO, Inc. Dr. Barber, formerly with The Australian National University, is presently at the Research Institute, University of Dayton, Dayton, Ohio. The manuscript (ARO Control No. ARO-VKF-TR-75-143) was submitted for publication on September 15, 1975.

The author gratefully acknowledges the assistance of John Miller in conducting the investigation and preparing this report and the support of Glenn Norfleet and John Cable throughout the study.

CONTENTS

	<u>Page</u>
1.0 INTRODUCTION	
1.1 Rail Gun	7
1.2 Reentry Conditions	8
2.0 OPERATIONAL ENVELOPE FOR RAIL GUN	
LAUNCHING AND SUSTAINING	
2.1 Accelerating Force	8
2.2 Ohmic Heating	13
2.3 Electromagnetic Stability	17
2.4 Contact Phenomena	17
2.5 Driving Methods	26
3.0 APPLICATIONS	
3.1 Launcher	32
3.2 Sustainer	47
4.0 CONCLUSIONS	
4.1 Launcher	74
4.2 Sustainer	75
REFERENCES	76

ILLUSTRATIONS

Figure

1. Simple Rail Gun	7
2. Practical Rail Geometry	10
3. L' and α as Functions of W/h for Rectangular Rails- High Frequency Limit	11
4. Possible Launch Package Configuration	12
5. Acceleration Current as a Function of Accelerated Mass for $L' = 0.6 \mu H/m$ and Various Accelerations, "a"	13
6. Resistive Heating Envelopes for Rail Gun Acceleration	15
7. Schematic of Resistive Heating Envelopes for Rail Gun Acceleration	16

<u>Figure</u>	<u>Page</u>
8. Electrical Wear versus Accelerator Length for Copper at Constant Acceleration to 6 km/sec	24
9. Projectile Wear versus Launch Mass for Various Values of Friction Coefficients, μ	27
10. Efficiency and Relative Velocity versus Inductance	31
11. Maximum Launchable Mass versus Rail Height	35
12. Velocity versus Accelerator Length	36
13. Efficiency and Acceleration Ratio versus $L_0/L'x$	40
14. Efficiency versus Acceleration Ratio	40
15. Stored Energy versus Projectile Diameter	41
16. Rail Gun Restraining Structure	43
17. Estimated Gun Cost versus Size	44
18. Possible Launch Package Geometry	46
19. Projectile Contact Detail	46
20. Possible Improved Contact Leaf	46
21. Relative Velocity versus Flight Distance	48
22. Relative Sustaining Energy versus Flight Distance	49
23. Drag Energy Loss Ratio versus Ballistic Coefficient	50
24. Sustaining Energy Ratio versus Projectile Diameter	51
25. Sustaining Energy versus Projectile Diameter	52
26. Relative Sustaining Force versus Flight Distance	53
27. Sustaining Force Profiles for Reentry Simulation	54
28. Relative Maximum Sustaining Energy versus Range Length	55
29. Sustainer Rail Geometry	56
30. Ohmic Heating Limitations	59
31. Circuit for Capacitively Driven Sustainer	64

<u>Figure</u>	<u>Page</u>
32. Sustaining Forces for Capacitively Driven Sustainer	66
33. Effect of Capacitance on Sustaining Force	68
34. Sustaining Force versus Relative Distance with Resistive Losses	68
35. Energy Efficiency versus Sustainer Length	69
36. Force Profiles for Various Capacitances	69
37. Stored Energy versus Range Length	70
38. Possible Restraining Structure	72
39. Cost Per Sustainer	74
NOMENCLATURE	78

1.0 INTRODUCTION

1.1 RAIL GUN

An electromagnetic rail gun consists essentially of two conducting rails (electrodes) between which a conducting projectile is placed. Electric current is passed down one electrode, through the projectile, and back along the other electrode (Fig. 1). The current, I , flowing through the projectile interacts with the magnetic flux resulting in an $I \times B$ force in the direction indicated.

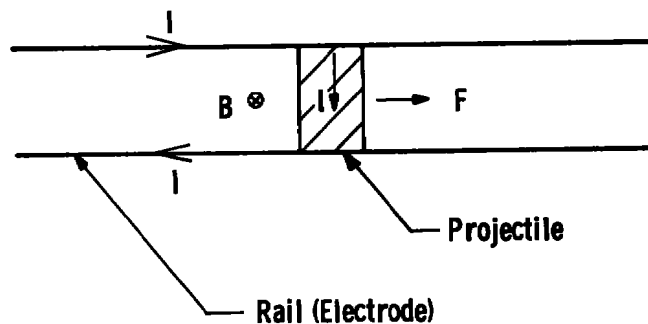


Figure 1. Simple rail gun.

The magnetic flux density B resulting from the rail currents may be augmented or entirely replaced by an externally generated magnetic field. However, only the simple case using rail-generated fields will be considered in this report.

As the projectile is free to slide along the rails, it will be accelerated by the $I \times B$ force as long as current continues to flow in the circuit and the projectile remains in electrical contact with the rails.

Millsaps and Pohlhausen (Ref. 1) examined the detailed behavior of a restricted class of rail guns in 1960. Their study was confined to a computer simulation of various capacitor-driven configurations. Chapman et al. (Ref. 2) describe a rail gun in which an explosively compressed magnetic field was used. It was reported to have projected a "coherent luminous cloud" at 10.5 km/sec. Braste and Sawle (Ref. 3) employed a capacitor bank to drive what was essentially a plasma rail gun and used the high velocity plasma generated to drag accelerate small (0.0024 g) nylon spheres to 6 km/sec. Sawle (Ref. 4) describes a variation of this arrangement which employs

plasma drag to accelerate even smaller ($\sim 35 \mu g$) glass spheres to 15 km/sec. Barber (Ref. 5) constructed a relatively large inductively driven rail gun and has launched solid projectiles of 2-g mass to 2 km/sec.

The purpose of this report is to examine the feasibility of using the rail gun acceleration principle in launching and/or velocity sustaining of large (> 20 -cm diam) reentry vehicle models. The report will develop theoretical rail gun principles, then apply them to the immediate reentry vehicle problem. The feasibility of the use of rail gun acceleration for launching and/or velocity sustaining of reentry models will then be assessed.

1.2 REENTRY CONDITIONS

To obtain experimental measurements of the behavior of reentry vehicles it is necessary to duplicate expected reentry conditions in the laboratory. Briefly the reentry conditions to be investigated in this report are:

1. Reentry velocity of 6 km/sec
2. Model sizes of from 20 to 40 cm in diameter
The larger the model that can be tested, the more reliable the data will be when transferred to actual reentry vehicles.
3. Ballistic coefficients (β) of from 50 kN/m^2 (1,000 lb/ft²) to 150 kN/m^2 (3,000 lb/ft²)
The higher β models (150 kN/m^2) are of most interest and will be used as the "datum" for comparison of performance.

2.0 OPERATIONAL ENVELOPE FOR RAIL GUN LAUNCHING AND SUSTAINING

2.1 ACCELERATING FORCE

Consider any inductive circuit of inductance L carrying current I . The magnetic energy $E = LI^2/2$ stored in the circuit and the magnetic flux $\phi = LI$ are both conserved as the time of observation reduces to

zero. Therefore, the instantaneous force on each element of the circuit may be expressed as

$$\begin{aligned}\vec{F} &= \nabla E \\ &= \nabla LI^2/2 \\ &= \frac{I^2}{2} \nabla L\end{aligned}$$

In the case of a linear rail gun, the inductance of the gun is $L'x$ where L' is the inductance per unit length of the gun and x is the projectile position from the breech. The force on the projectile may then be expressed as

$$F = L'I^2/2$$

The force on a projectile in a rail gun is therefore a function only of the inductance per unit length of the rails (a geometrical factor) and the current flowing in the system. The force does not depend on current distribution in the projectile or rails (except for the usually negligible change this produces in L') or on the mass or shape of the projectile.

The acceleration may be obtained by simply dividing the force by the mass

$$a = L'I^2/2m \quad (2.1)$$

To ensure that all sections of the projectile experience the same acceleration force it is desirable to have a uniform magnetic field across the projectile and a uniform current density in the projectile. If the field or current density varies from one part of the projectile to another, it will experience differential accelerations and will be stressed or deformed. A number of rail geometries such as coaxial, parallel round bars, or parallel flat bars might be considered. Each geometry can only approximate the desired conditions. For example, the magnetic field in a coaxial system has a $1/r$ dependence and becomes radially uniform as the annular gap between the electrodes reduces to zero. Similarly, with a parallel flat conductor system the field becomes uniform as the gap between the rails reduces to zero. The application considered herein probably eliminates the annular projectiles required for coaxial geometries, and the most practical rail geometry appears to be parallel flats with a notionally "rectangular" projectile (Fig. 2).

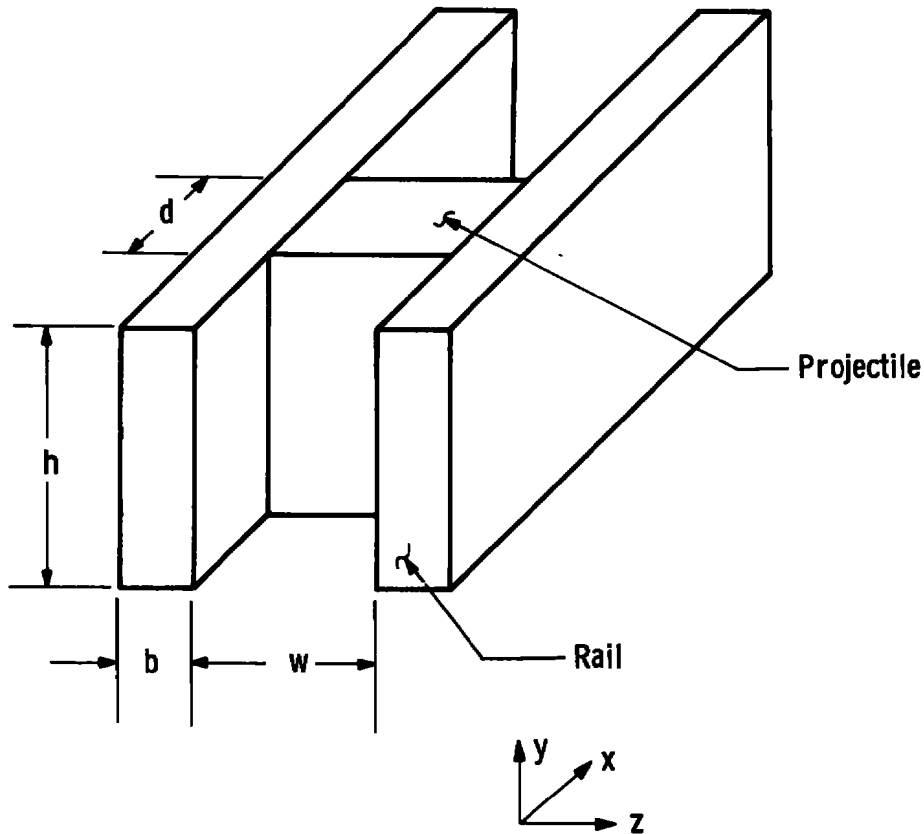


Figure 2. Practical rail geometry.

The inductance L' of the rectangular rails shown in Fig. 2 is a function of the ratio w/h and to some extent the ratios b/h and b/w . In the high frequency approximation all the current flows at the inside surface of the rails and the effective rail thickness, b , is zero. Approximately 90 percent of the accelerating field B at the projectile is generated by currents in only two or three rail gap widths, w , back along the rails. When the projectile is at even moderate velocities, the current in this part of the rails does not have time to diffuse into the rails and the high frequency inductance is therefore the most appropriate one to calculate. We shall, therefore, assume $b = 0$ in calculations of rail inductance.

Considering the rails as current sheets, the magnetic flux density in the immediate vicinity of the rails is given by

$$B = \mu_0 \phi l' / h$$

If the field is uniform across the rail gap, then the magnetic flux per unit length of rails ϕ' is given by

$$\begin{aligned}\phi' &= L'I = Bw \\ &\sim \mu_0 \phi I w/h\end{aligned}$$

which, on elimination of I , provides

$$L' \sim \mu_0 \phi w/h$$

A better calculation of inductance can be obtained using formulas developed by Grover (Ref. 6) and these are shown as a function of w/h in Fig. 3. Also shown is the ratio of calculated inductance L' (from Grover) to the uniform field inductance $L' = \mu_0 w/h$. This ratio is an indication of the uniformity of the magnetic field across the projectile (in the z direction) and is a figure of merit for the geometry. A uniformity ratio of unity indicates a highly uniform magnetic field and therefore a "good" geometry while a uniformity of zero indicates a nonuniform field (actually $B = 0$ halfway across the gap) and a "bad" geometry. (if the projectile is sufficiently strong and/or the acceleration is low, a "bad" geometry could be tolerated.)

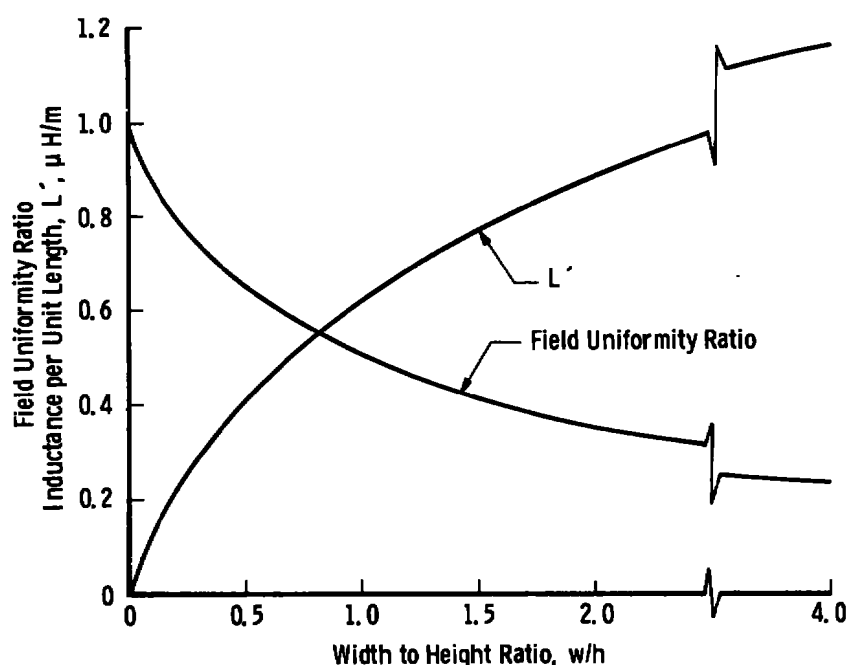


Figure 3. L' and α as functions of W/h for rectangular rails—high frequency limit.

Because of the requirement of launching an axially symmetric model, a geometry approaching that of "square" (i.e., $w/h \approx 1$) is probably the most appropriate as this permits efficient use of projectile material for a given size model as shown in Fig. 4. From Fig. 3 it is apparent that appropriate values of L' therefore lie in the range of $0.6 \mu H/m$.

In this report, "projectile" will refer only to the driving portion of the "launch package." The "projectile" together with the "model" make up the total "launch package" as shown in Fig. 4.

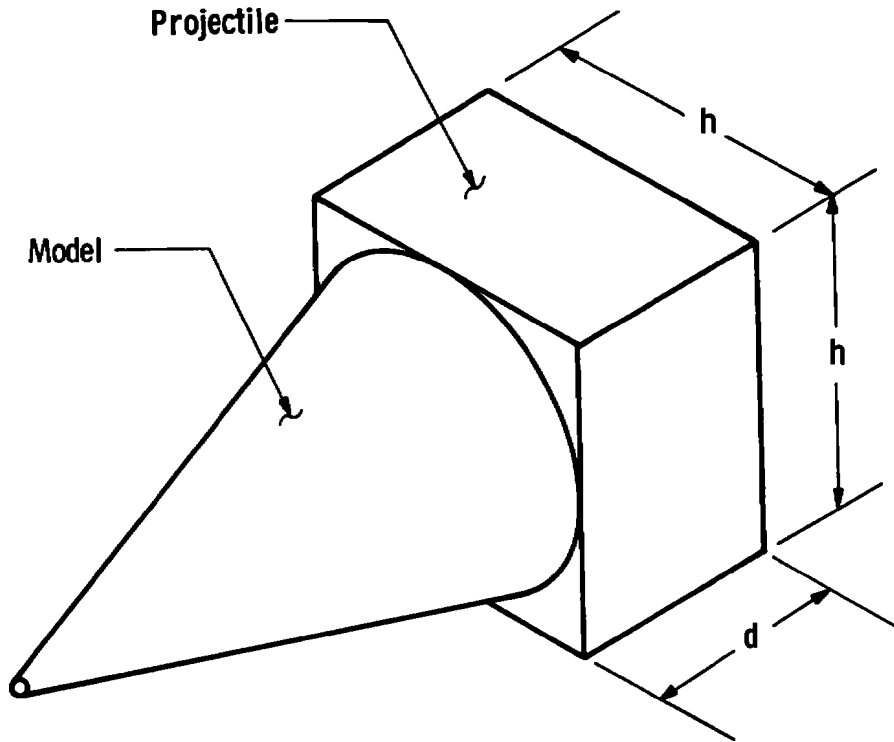


Figure 4. Possible launch package configuration.

Using the previously derived acceleration formula Eq. (2.1) we can derive the current-acceleration relation

$$I = (2 m a' L')^{1/2} \quad (2.2)$$

Results are displayed in Fig. 5 for $L' = 0.6 \mu\text{H/m}$.

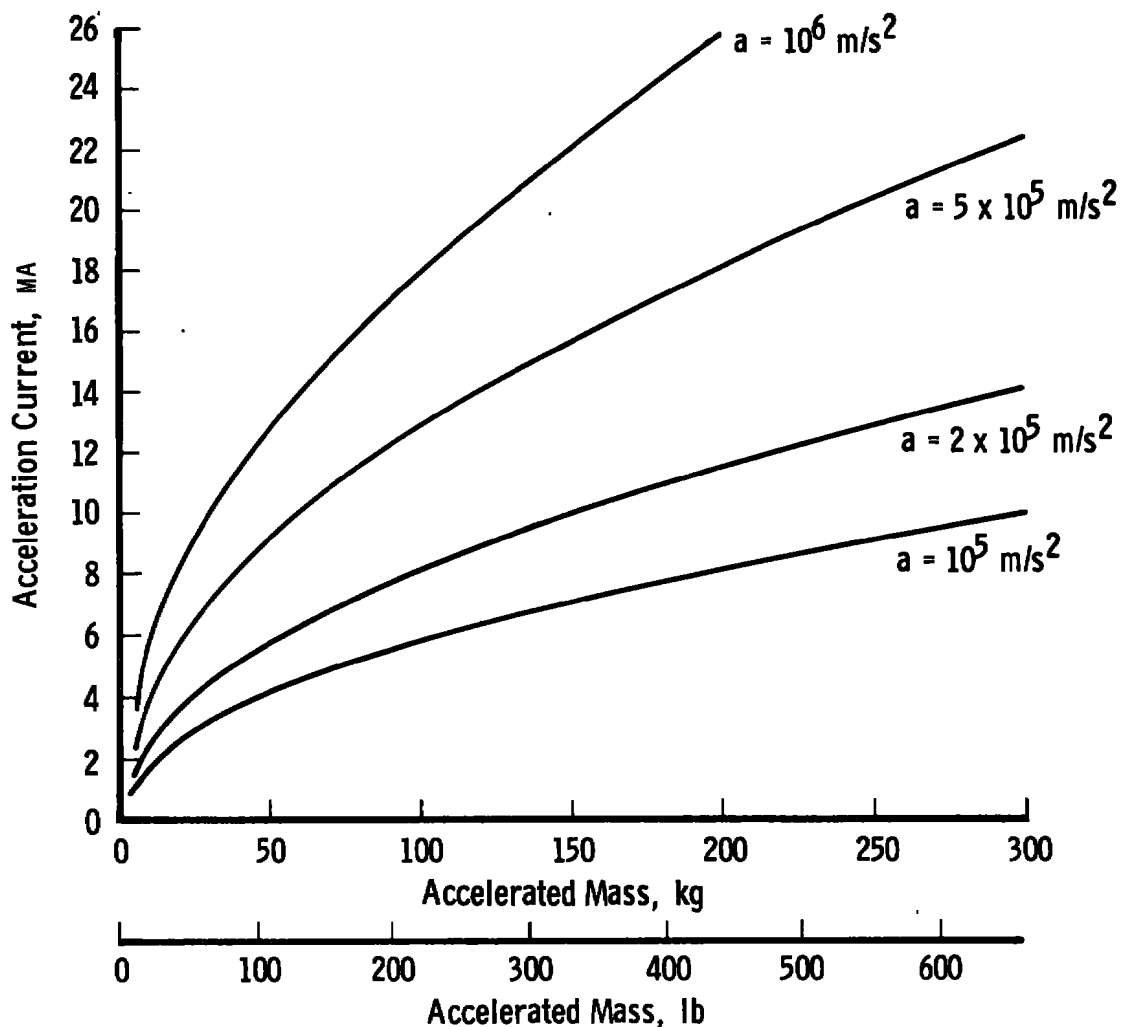


Figure 5. Acceleration current as a function of accelerated mass for $L' = 0.6 \mu\text{H/m}$ and various accelerations, "a".

2.2 OHMIC HEATING

The projectile portion of the launch package must carry the acceleration current and consequently experiences resistive or ohmic heating effects. Assuming that the current density is uniform, we may write the action integral as (Ref. 7)

$$\int I^2 dt = g_1 A^2$$

where I is the total current flowing, g_1 is the action constant which is a function of the material and its state (temperature), and A is the current-carrying cross-sectional area of the projectile. From the acceleration formula Eq. (2.1) we can write the velocity as

$$\begin{aligned} v &= \int \frac{L' I^2}{2m} dt \\ &= \frac{L'}{2m} \int I^2 dt \end{aligned}$$

assuming that both L' and m remain constant during acceleration. These two equations can then be combined to yield

$$v = L' g_1 A^2 / 2m \quad (2.3)$$

(It should be noted that this equation also holds incrementally (i. e., $\Delta v = L' A^2 \Delta g_1 / 2m$)).

Referring to Fig. 2 we note that the current-carrying cross-sectional area of the projectile is $A = hd$. The projectile thickness, d , cannot be arbitrarily large because of the electrical skin effect. In order that the action integral ($\int I^2 dt$) be a realistic measure of energy dissipated in the projectile, the current density I/A must be uniform, or approximately so, throughout the projectile during acceleration. Electric current diffuses into a conductor but for short times is restricted to the surface or "skin" of the material. The depth to which current diffuses in a given time is called the electrical skin depth, δ , and is given by

$$\delta = \sqrt{\pi \zeta t / \mu_0}$$

where ζ is the electrical resistivity of the material and t is the time. Therefore, in a rail gun, the temperature described by the action integral will be valid for some thickness of conductor less than the skin depth for the time of acceleration. We shall choose $d = 0.5\delta$ (i. e., the current density in this thickness is essentially uniform for 75 percent of the acceleration time). Therefore,

$$d = 0.5\sqrt{\pi \zeta t / \mu_0}$$

or

$$A = hd = 0.5h\sqrt{\pi\zeta t/\mu_o}$$

The representative acceleration time, t , may be obtained from the desirable case of constant acceleration as $2x/v$, and

$$A = 0.5h\sqrt{2\pi\zeta x/\mu_o v} \quad (2.4)$$

Equations (2.3) and (2.4) are shown plotted in Fig. 6 for copper. Copper was chosen as it is a suitable acceleration material combining high heat capacity and low electrical resistivity.

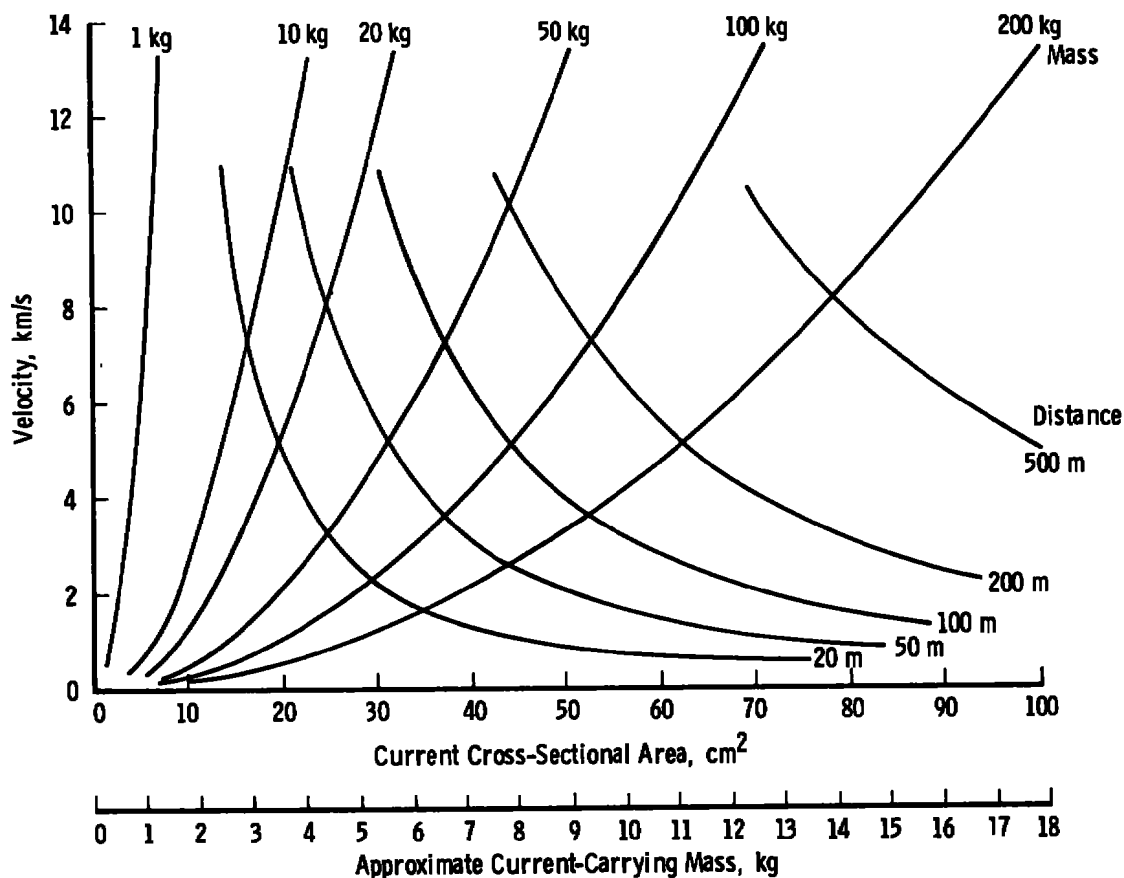


Figure 6. Resistive heating envelopes for rail gun acceleration.

Equation (2.3) appears as the constant accelerated mass lines. The region above these lines corresponds to at least partial melting of the projectile. The parameter values used were

$$L' = 0.6 \mu\text{H/m}$$

$$g_1 = 8.9 \times 10^{16} \text{ A}^2\text{-sec/m}^4 \text{ (Cnare, Ref. 7, for copper at the melting point)}$$

Equation (2.4) is represented in Fig. 6 by the constant acceleration distance lines. The region above the lines corresponds to partial melting, while that below is "safe." The values used in Eq. (2.4) were

$$h = 20 \text{ cm}$$

$$= 2 \times 10^{-8} \Omega\text{-cm (copper)}$$

Figure 6 may be interpreted as illustrated in Fig. 7. For reliable operation an accelerator would probably have to operate in the "safe" region. For example, if a velocity (say 6 km/sec) and a mass (say 50 kg) are chosen, a minimum gun length of approximately 100 m is required.

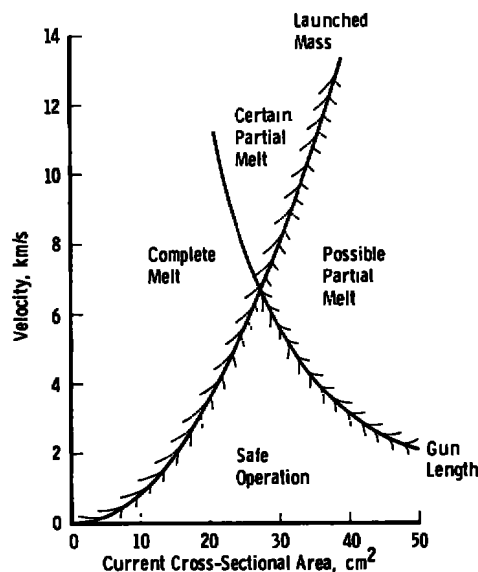


Figure 7. Schematic of resistive heating envelopes for rail gun acceleration.

It might be noted that increasing h (the projectile height) increases the mass that can be accelerated with a given length of gun.

2.3 ELECTROMAGNETIC STABILITY

There are basically two modes of electromagnetic instability in a rail gun:

1. The Rayleigh-Taylor instability. This is the tendency for the projectile to "cock" in the barrel or to "blow out" through the center.
2. The vertical instability. The projectile, if it moves out of the center of the rails perpendicular to the direction of acceleration, will tend to continue to move out of the rails.

The Rayleigh-Taylor instability occurs in solids only at high acceleration where the solid behaves in a fluid manner, and it would not be expected to occur at the low accelerations considered in this study. Although "cocking" may tend to occur at low acceleration, the projectile will behave as a rigid body and it is possible to make it stable against cocking by, for example, making it relatively long ($d/w > 1$).

The vertical instability is a case of neutral stability, that is, if the projectile is maintained at or near the center of the rail system, the instability force will be small. It is possible to provide mechanical restraint to this mode of instability by, for example, "closing" the barrel with insulating spacers on the top and bottom of the rails.

2.4 CONTACT PHENOMENA

The behavior of contacts can be divided into two aspects, (1) mechanical behavior and (2) electrical behavior. The two are related as will be shown later, but it is helpful to begin the discussion with the separation. These two aspects can be further divided into static and dynamic behavior, and this will be done for both mechanical and electrical behavior. Finally, contact wear will be considered.

2.4.1 Mechanical Behavior

(a) Static Behavior

When two solids are brought into contact, they first meet at the highest interfering asperities on the surfaces (the surfaces being microscopically rough). As the normal load on the interface is increased, the interfering asperities are crushed down and the area of interference increases. Lower asperities begin to interfere as the surfaces move closer together and the number of interfering asperities increases. Finally, with sufficient normal force, the entire surface comes into intimate contact.

Two phenomena characterize the mechanical behavior of solid/solid contacts, friction and wear. Both can be formulated in simple analytic terms.

Consider the nominal contact area to be A and the area of actual metal to metal contact A_b (sometimes referred to as the load bearing area). The ratio of $A_b/A \leq 1$. The load bearing area A_b can be related to the normal load P in the contact by

$$P = \sigma A_b$$

where σ is an average yield stress in the areas of true contact. σ is related to the bulk properties of the material and is treated in detail by Bowden and Tabor (Ref. 8). Let us suppose that the area A_b is made up of n identical contacts of area A_{bn} ; then

$$P = n\sigma A_{bn} \quad (2.5)$$

Thus, as P increases, A_{bn} increases and/or n increases (σ is a material property and remains constant).

The area of contact A_b is in intimate contact and cold welding of the surfaces at these points will occur. If the surfaces are moved tangentially, these welds must be broken. The tangential force S required to accomplish this is

$$S = sA_b$$

where s is the shear strength of the material. Thus the coefficient of friction may easily be shown to be

$$\mu_f = S/P = s/\sigma$$

This very simple picture of friction is adequate for this discussion. (A more detailed discussion is contained in Ref. 8).

Wear occurs with the assymetrical shearing of the cold welded areas A_{bn} . In principal, two identical material surfaces will not experience any net wear except for wear particles which are dislodged from both surfaces. Different materials and different states of the same material in contact will undergo net wear and the particular case must be considered to determine which surface will wear and by how much.

(b) Dynamic Behavior

As the rubbing velocity is increased from zero (static), the simple picture of friction and wear developed above essentially still holds. However, sliding affects both the contact area A_b and the material properties σ and s .

At low sliding speeds (<10 m/s), the dynamic case is identical to the static case. Shearing of the local contacts takes place slowly enough that thermal equilibrium is established and the material properties do not change. The contact area A_b grows slightly due to the vector nature of the stresses σ and s (i.e., the vector resultant stress determines the maximum stress and as this is greater than either σ or s , the area must grow to return the average stress to the yield value—see Bowden and Tabor, Ref. 8). As the velocity of sliding increases, the sheared areas A_b depart from thermal equilibrium because the energy liberated from the shearing does not have time to conduct into the bulk of the material. The shearing volume thus experiences a temperature rise and a resultant lowering of the shear strength s . There is little effect on the compressive yield stress σ so wear and the coefficient of friction decrease. They both continue to fall as velocity is increased until the whole surface is covered by a molten film. The coefficient of friction is then determined by the velocity gradient in the molten layer and the viscosity of the liquid. As velocity is further increased, the molten layer contracts in thickness

and friction and wear begin to increase. Bowden and Tabor (Ref. 8) found that the minimum for copper on steel occurred at greater than 700 m/sec at which velocity the coefficient of friction was remarkably low ($\mu_f = 0.2$).

As 700 m/sec is barely in the range of interest here, one might wonder what happens as velocity is further increased. To the author's knowledge, there are no coefficient of friction data available and very few observations of any type at higher velocities on intimately touching sliding contacts. Graff and Detlaff (Ref. 9) reported the gouging phenomena on high-speed rocket sled rails (up to 1,500 m/sec) and Barber (Ref. 5) confirmed the phenomena in a rail gun. This phenomena involves the formation of tear shaped "craters" on the surface of the rails. It only occurs at high velocities (> 600 m/sec for copper on copper) and is very incompletely understood. The author feels it is a hypervelocity impact effect (i. e., the material behaves as a fluid) and may be caused by discrete asperity impacts or by a basic fluid instability (Kelvin-Helmholtz) at the fluid boundary. No good measure of the coefficient of friction or of wear is available above a few hundred meters per second. The apparent violence of the gouging phenomena would indicate high wear rates, but Barber (Ref. 5) has found some evidence that gouging ceases at very high velocities (≥ 1.1 km/sec for copper on copper). Graff and Detlaff (Ref. 9) and Barber (Ref. 5) have found that rail coatings can produce a marked reduction of gouging.

2.4.2 Electrical Behavior

(a) Static Behavior

The principal electrical feature of contacts is the constriction of the current flowing across the contact into the areas of real contact A_b . It is this constriction of current which gives rise to the important electrical effects at the contact interface.

Holm (Ref. 10) has shown that the equivalent resistance of a circular contact area of radius "r" between two surfaces is approximately

$$R = \zeta / 2r$$

where ζ is the electrical resistivity. If we consider again n identical contacts of area A_{bn} , the equivalent resistance is that of n individual contacts in parallel, or

$$\zeta / (2n \sqrt{A_{bn}} / \pi)$$

A_{bn} may be replaced from Eq. (2.5) as $A_{bn} = P/n\sigma$ to yield

$$R = (\zeta/2)(\pi\sigma/Pn)^{1/2} \quad (2.6)$$

In order to pass large currents, such as envisioned in this report, low contact resistance is required; therefore, low resistivity-low yield strength materials with high normal forces and a large number of individual contacts are required.

The passage of current through the constricted areas A_b generates resistive heat in the contacting asperities. It has been demonstrated (Ref. 10) that the maximum temperature in the contact and the voltage developed across the contact are related. That is, the voltage is a measure of the contact temperature and vice-versa. For example, in copper the melting point is reached at about 0.4 volts and the boiling point is reached at 0.8 volts. Bowden and Williamson (Ref. 11) have shown that, provided the surfaces are free to move together as current is increased through a contact, the voltage across the contact (and thus temperature at the contact) tend to be a constant value. As current is increased, the contact heats slightly and collapses to a larger area which reduces the current density and resultant heating. If a certain critical voltage (temperature) across the contact is exceeded the contact becomes unstable, heats rapidly, and explodes.

(b) Dynamic Behavior

The effect of rubbing velocity on the electrical behavior of contacts has not received much attention above about 100 m/sec. Barber (Ref. 5) in rail gun experiments has found that for copper on copper and a particular geometry, good contact (contact voltage <0.5V) can be maintained up to over 1 km/sec; however, instability sets in at higher velocities. The process of instability initiation and growth is not understood at present, but the contact appears to suddenly change from metal to metal contact to an arcing contact.

In a rail gun the projectile moves continuously onto cold rails, the effect of which will be to cool the contacts and also to wipe away any molten material. As contact voltage (temperature) increases, increased wear might be expected. No good data are available.

Gouging does not appear to affect electrical contact, that is, electrical behavior appears to be independent of the gouging processes. Gouging does not necessarily coincide with poor electrical contact.

2.4.3 Contact Wear

Contact wear may be considered as two separate phenomena, electrical wear and mechanical or frictional wear. They may, of course, be interactive but for the purposes of this analysis will be treated separately.

(a) Electrical Wear

The electrical resistance of a contact surface is, in general, higher than that of the bulk of the material due to current constriction through the contact spots and heating of the contact area by the current. The contact can be characterized electrically by a contact voltage V (as pointed out previously this voltage is also an indication of contact temperature). If the contact carries an average current density, i , then the average power density dissipated in the contact is

$$W = Vi$$

Now let us assume that this power is liberated in a very thin contact region and that it melts the material in that region. (Note: melting is consistent with $V = 0.5$ V.) We then assume that in a sliding contact, the molten material is wiped (worn) away. The amount of material worn away (per unit area) may be described in terms of the wear δ_w . If the energy required to melt the material is Q_m (per unit volume) then the melting power density is related to the wear rate by

$$W = Q_m d\delta_w/dt$$

which may be equated to the electrical dissipation

$$Q_m d\delta_w/dt = Vi$$

In the case of a rail gun, the projectile wear is of most interest. Only a fraction of the energy will be dissipated in the projectile and as the projectile continually runs onto cold rails, the maximum fraction would be one-half. So for the projectile

$$Q_m d\delta_w/dt = \frac{1}{2} Vi$$

or

$$\delta_w = \int_0^t \frac{V_i}{2Q_m} dt$$

Assuming that the contact voltage is constant for the time of interest, then

$$\delta_w = \frac{V}{2Q_m} \int i dt$$

For a constant acceleration, the current is constant and current density i can be extracted from the mass and acceleration as follows:

From resistive heating (Eq. (2.3)) we obtain the limiting velocity

$$v = L' g_1 A^2 / 2m$$

or

$$A = (2mv/L'g_1)^{1/2}$$

From the acceleration (Eq. (2.2))

$$I = (2ma/L')^{1/2}$$

Therefore

$$i = I/A = \left(\frac{g_1 a}{v} \right)^{1/2}$$

Now for a constant acceleration $a = v^2/2x$, $t = 2x/v$, and

$$\int i dt = \left(\frac{2g_1 x}{v} \right)^{1/2}$$

Thus, the wear becomes

$$\delta_w = \frac{V}{2Q_m} \left(\frac{2g_1 x}{v} \right)^{1/2}$$

For copper $Q_m \approx \rho c_p \Delta T_m \approx 3.6 \times 10^9 \text{ J/m}^3$

$$g_1 \leq 8.9 \times 10^{16} \text{ A}^2\text{-sec/m}^4$$

Wear versus gun length is plotted in Fig. 8.

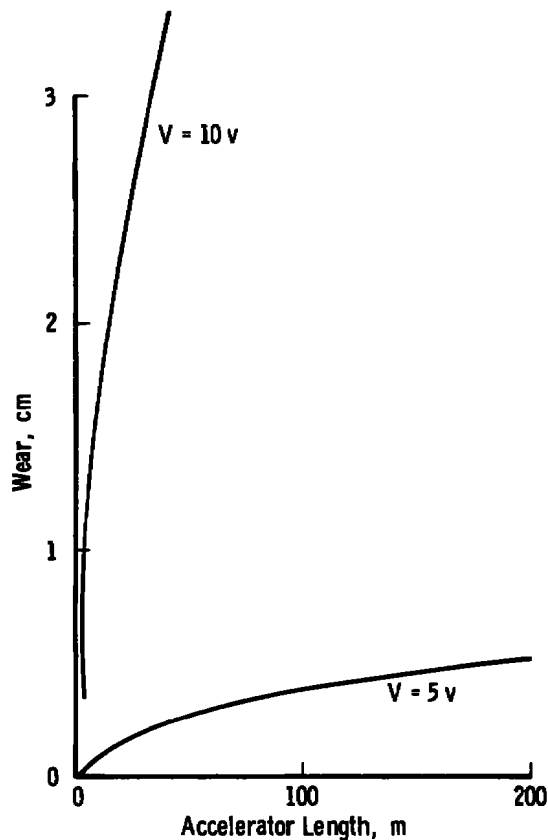


Figure 8. Electrical wear versus accelerator length for copper at constant acceleration to 6 km/sec.

(b) Mechanical/Frictional Wear

The frictional force dissipates energy in the contact region and may also result in melting and wear of the contact. The frictional force is related to the normal force by the coefficient of friction μ_f

$$F_f = \mu_f P$$

Thus the total energy dissipated by the frictional force may be written as

$$\int F_f dx = \int_0^x \mu_f P dx$$

or the dissipation energy density as

$$\int_0^x \mu_f \frac{P}{A} dx$$

where P/A is simply the average compressive stress at the interface. If the interface material is melted by friction and removed by wiping we can again equate the dissipative energy density to a wear δ_w , where one-half the energy goes into the projectile, and one-half into the rails

$$Q_m \delta_w = \frac{1}{2} \int \mu_f P/A dx$$

$$\delta_w = \frac{1}{2Q_m A} \int \mu_f P dx$$

The normal force P cannot be arbitrarily small; it must be large enough to ensure good electrical contact. The contact resistance R can be written as (Eq. (2.6))

$$R = \left(\frac{\zeta}{2}\right) \left(\frac{\pi \sigma}{P n}\right)^{1/2}$$

Thus the contact voltage V is

$$V = IR$$

or

$$R = V/I$$

and

$$P = \zeta^2 I^2 \pi \sigma / 2n V^2$$

The normal load must be at least equal to this value to ensure good contact. Thus δ_w becomes, for a constant friction coefficient

$$\begin{aligned}\delta_w &= \frac{\mu_f}{2Q_m A} \int P \, dx \\ &= \left(\frac{\mu_f}{2Q_m A} \right) \left(\frac{\pi \sigma \zeta^2}{2n V^2} \right) \int I^2 \, dx\end{aligned}$$

Now for constant acceleration, $\int I^2 dx = mv^2/L'$ (i. e. $a = L'I^2/2m$), therefore

$$\delta_w = \left(\frac{\mu_f}{2Q_m A} \right) \left(\frac{\pi \sigma \zeta^2}{2n V^2} \right) \left(\frac{mv^2}{L'} \right)$$

Frictional wear depends on the final kinetic energy of the launch package and on various material properties. Figure 9 shows the expected wear for the following characteristic parameters

$$\begin{aligned}Q_m &= 3.6 \times 10^9 \text{ J/m}^3 \text{ (copper)} \\ A &= 10 \times 10^{-4} \text{ m}^2 \\ \sigma &= 2 \times 10^8 \text{ nt/m}^2 \\ \zeta &= 2 \times 10^{-8} \text{ r-m} \end{aligned} \left. \vphantom{\begin{aligned}Q_m \\ A \\ \sigma \\ \zeta\end{aligned}} \right\} \text{copper}$$

$$\begin{aligned}V &= 0.5 \text{ v ("melting" voltage for copper)} \\ n &= 5,000 \text{ (number of contact fingers)} \\ v &= 6 \times 10^3 \text{ m/sec}^2 \\ L' &= 0.6 \mu\text{ll/m}\end{aligned}$$

Gouging might be expected to contribute to wear but no data are available on this aspect of the phenomena. An important consideration of gouging is rail damage and the associated necessity to replace or dress the rails after each shot.

2.5 DRIVING METHODS

There are basically two methods of storing electrical energy and subsequently driving a rail gun, (1) capacitors and (2) inductors. Both of these methods will be considered.

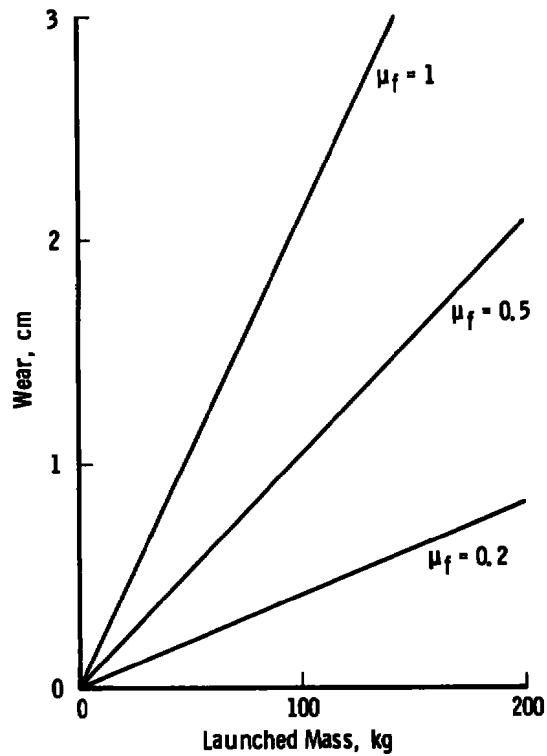
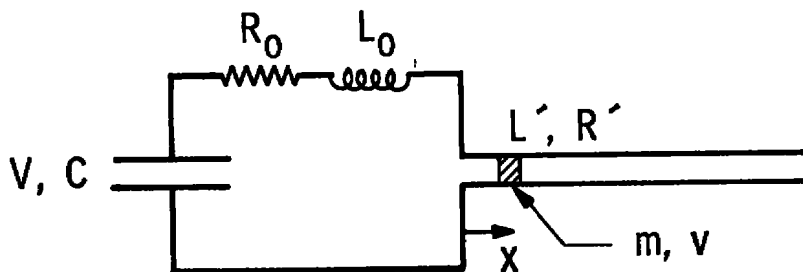


Figure 9. Projectile wear versus launch mass for various values of friction coefficients, μ .

2.5.1 Capacitor Driving

A capacitor-driven rail gun may be represented as:



The equations which describe the operation of this circuit are

1. Conservation of Energy

$$(1/2)CV_0^2 = 1/2 CV^2 + 1/2 mv^2 + 1/2(L_0 + L'x)I^2 + \int I^2(R_0 + R'x) dt + \int F_d x dt$$

2. Voltage Around the Circuit

$$V_o = \frac{1}{C} \int I dt + I(R_o + R'x) + \frac{d}{dt} \{(L_o + L'x)I\}$$

3. Dynamic Equations

$$a = L'I^2/2m - F_d/m$$

$$v = \int a dt$$

$$x = \int v dt$$

For a frictionless system in a vacuum, the retarding force F_d is zero. These equations together are nonlinear and must be solved numerically; however, a better understanding of the general system behavior is obtained from an approximate analytic solution. The approximations used are

$$C \rightarrow \infty \text{ (i.e., a battery or very large capacitor)}$$

$$R_o \text{ and } R' \rightarrow 0 \text{ (i.e., neglect resistive losses)}$$

With these approximations, the energy equation implies $V_o = V = \text{constant}$. The voltage equation reduces to

$$V = \frac{d}{dt} (L_o + L'x)I$$

which can be easily integrated to yield

$$Vt = (L_o + L'x)I$$

The force on the projectile may then be written as

$$F = \frac{L'}{2} \left(\frac{V_o t}{(L_o + L'x)} \right)^2$$

or

$$F = \frac{L'}{2} \left(\frac{V_o}{(L_o/t + L'\bar{v})} \right)^2$$

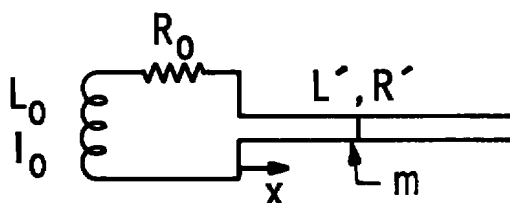
where $\bar{v} = x/t$, is some measure of the average velocity. From this equation it should be noted that:

1. At low velocities (\bar{v}) the accelerating force is large ($F \rightarrow \infty$ as $\bar{v} \rightarrow 0$ if $L_0 = 0$), and at high velocities F becomes small. That is, capacitor drive produces a basically nonuniform acceleration.
2. If L_0 is negligibly small ($L_0 \ll L'x$) then the accelerating force is proportional to $(V_0/\bar{v})^2$. That is, if a projectile is, for example, fired at velocity v into a capacitor-driven gun, the voltage may be adjusted to provide any required force (F). If the velocity remains constant, then F will also remain approximately constant.

These aspects will be considered in more detail later, but the important point to keep in mind is that capacitors produce an acceleration which basically varies as $1/v^2$.

2.5.2 Inductive Driving

The circuit of an inductively driven gun is as follows:



The equations that describe the system are:

1. Conservation of Energy

$$(1/2)L_0 I_0^2 = (1/2)(L_0 + L'x)I^2 + (1/2)mv^2 + \int I^2(R_0 + R'x) dt + \int F_d v dt$$

2. Conservation of Magnetic Flux

$$L_0 I_0 = (L_0 + L'x)I + \int I(R_0 + R'x) dt$$

3. Dynamic Equations

$$a = L'I^2/2m - F_d/m$$

$$v = \int a dt$$

$$x = \int v dt$$

For a frictionless system accelerated in a vacuum, the retarding force (F_d) is zero.

These equations together are nonlinear and must be solved numerically to obtain accurate results. However, a better general understanding of the system may be obtained by obtaining an approximate analytic solution. The approximation used is that

$$R_o + R'x \rightarrow 0 \text{ (i.e., a lossless system)}$$

Then the equations become

$$L_o I_o^2 = (L_o + L'x)I^2 + mv^2$$

and

$$L_o I_o = (L_o + L'x)I$$

which may be rearranged and solved to provide

$$v^2 = \frac{L_o I_o^2}{m} \left(\frac{L'x}{L_o + L'x} \right)$$

The energy efficiency (η) of the gun is

$$\left(\frac{mv^2}{L_o I_o^2} \right)$$

or

$$\eta = \frac{L'x}{L_o + L'x} = \frac{1}{1 + L_o/L'x}$$

and the velocity may be written as

$$v = \sqrt{\frac{L_o}{m}} \left(\frac{L'_x}{L_o + L'_x} \right)^{1/2} I_o$$

As the storage inductance (L_o) is increased, the velocity tends to a maximum v_{max}

$$v_{max} = (L'_x/m)^{1/2} I_o$$

Thus, the relative velocity $v_r = v/v_{max}$ as a function of storage inductance may be expressed as

$$v_r = \left(\frac{L_o/L'_x}{1 + L_o/L'_x} \right)^{1/2}$$

Both v_r and η are shown plotted in Fig. 10.

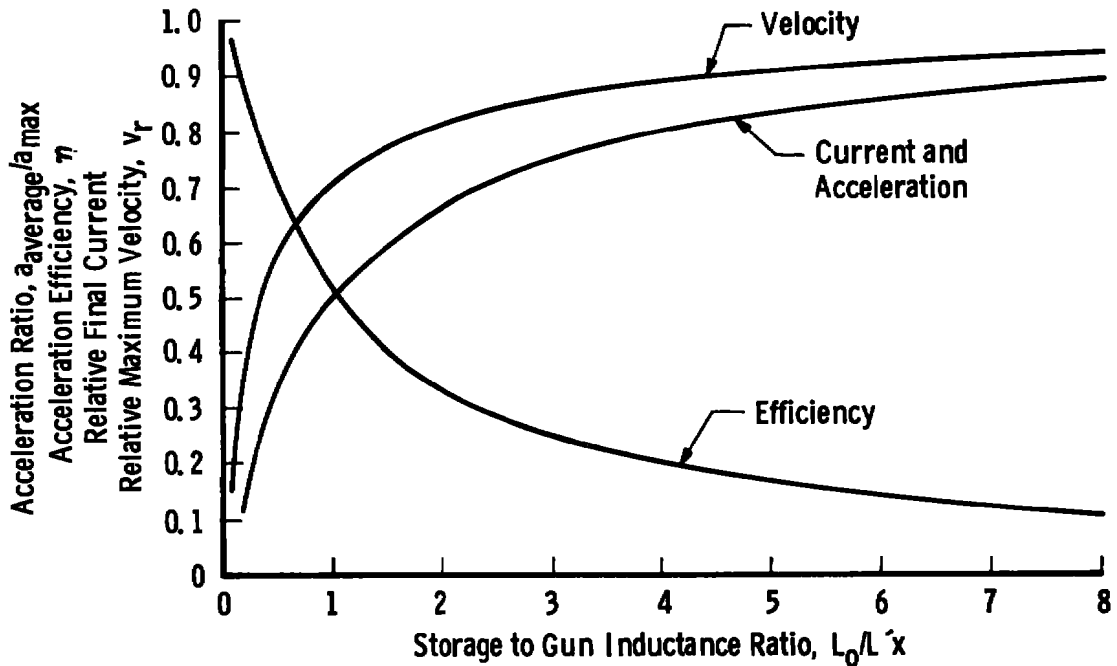


Figure 10. Efficiency and relative velocity versus inductance.

From Fig. 10 it is apparent that velocity must be traded off against efficiency. When losses are included, both efficiency and velocity might be expected to decline.

The current (I) can be expressed as

$$I = \left(\frac{L_o}{L_o + L'x} \right) I_o$$

or

$$\begin{aligned} I/I_o &= \frac{L_o}{(L_o + L'x)} \\ &= \frac{L_o/L'x}{1 + L_o/L'x} \end{aligned}$$

and this is also plotted in Fig. 10. As the final relative current approaches 1, this implies that the acceleration ($\propto I^2$) approaches a constant value. Thus, some choice must be made as to gun length, constancy of acceleration, and efficiency in order to determine the required storage inductance. Finally, a numerical solution must be carried out to determine the importance of resistive losses.

Figure 10 indicates that if a very large storage inductance is employed, the acceleration can be made extremely constant.

3.0 APPLICATIONS

3.1 LAUNCHER

The implications of the development of Section 2.0 will now be examined with respect to the use of a rail gun as a reentry vehicle model launcher. The envelope of rail gun performance to meet model launching requirements will be developed.

The principal technical constraints on a model launcher in order of importance are:

1. Reentry velocity [~ 6 km/sec] must be reached.
2. Adequate model size should be obtained [say 20 to 40 cm in diameter].

3. Ballistic coefficients ($mg/C_D A_R$) of up to 150 kN/m^2 ($3,000 \text{ lb/ft}^2$) should be reached to avoid sustaining.
4. Peak acceleration must be low ($\leq 200,000 \text{ m/sec}^2$).

These considerations will now be applied to the development of Section 2.0.

3.1.1 Model Acceleration

The required projectile shape essentially fixes the rail geometry. As pointed out in Section 2.1 and Fig. 2, an axially symmetric model suggests a square or almost square ($w = h$) rail geometry in order to optimize driving mass for a given model diameter. A square geometry has a high frequency inductance per unit length of rails of $\sim 0.6 \mu\text{H/m}$ independent of size (Fig. 3).

The force on the projectile may then be expressed as $L'I^2/2$ or the acceleration as $L'I^2/(2m)$. The acceleration therefore depends only on the current and mass as shown in Fig. 5. The $200,000\text{-m/sec}^2$ curve indicates the maximum current which can be employed as a function of launched mass.

For models with ballistic coefficients of 150 kN/m^2 , masses from approximately 50 kg (20-cm diam) to 200 kg (40-cm diam) are of interest. From Fig. 5 it can be seen that maximum currents of between 5 and 12 MA are therefore required if acceleration is not to exceed $200,000 \text{ m/sec}^2$.

Friction and aerodynamic drag could lower acceleration during launch; however, required acceleration could be attained by increasing the current to compensate. If the drag and frictional forces don't exceed about 20 to 30 percent of the acceleration force, then the additional current required should pose no heating problems.

3.1.2 Ohmic Heating

Ohmic heating considerations limit the choice of materials which might be used in a projectile to those having good electrical and thermal conductivity and good heat capacity (i. e., high action constant). Copper is such a material and has been chosen for this study.

Figure 6 indicates the regions of "safe" (nonmelt) operation from a resistive heating point of view. It is apparent that, for a given density,

as the mass increases the length of the accelerator must also increase. This may be formalized as follows:

From resistive heating considerations (Section 2.2)

$$A^2 = 2 m v / L' g_1$$

where g_1 is the action constant.

We can also write for a projectile of the shape shown in Fig. 2 that

$$A^2 = h^2 d^2$$

As previously noted, d is related to the skin depth by

$$d \approx 0.5 \sqrt{\pi \zeta t / \mu_0}$$

Assuming a constant acceleration, then $t = 2x_L / v$ and these equations may be combined to yield

$$m = \frac{0.25 \pi \zeta g_1 L' h^2 x_L}{\mu_0 v^2}$$

where x_L is the acceleration length.

The following values were substituted in the above equation with the results plotted in Fig. 11.

$$\begin{aligned} \zeta &= 2.0 \times 10^{-8} \Omega\text{-cm (copper)} \\ g_1 &= 6.0 \times 10^{16} \text{ A}^2\text{-sec/m}^4 \text{ (copper derated } \sim 30 \text{ percent} \\ &\quad \text{from melting)} \\ L' &= 0.6 \mu\text{H/m} \\ v &= 6 \times 10^3 \text{ m/sec} \end{aligned}$$

and therefore

$$m = 12.5 h^2 x_L \text{ (m in kg, h and } x_L \text{ in m)}$$

The curves in Fig. 11 represent the maximum masses that could be accelerated to 6 km/sec as a function of accelerator length and projectile diameter (rail height). Also shown is the desired $\beta = 150 \text{ kN/m}^2$ curve.

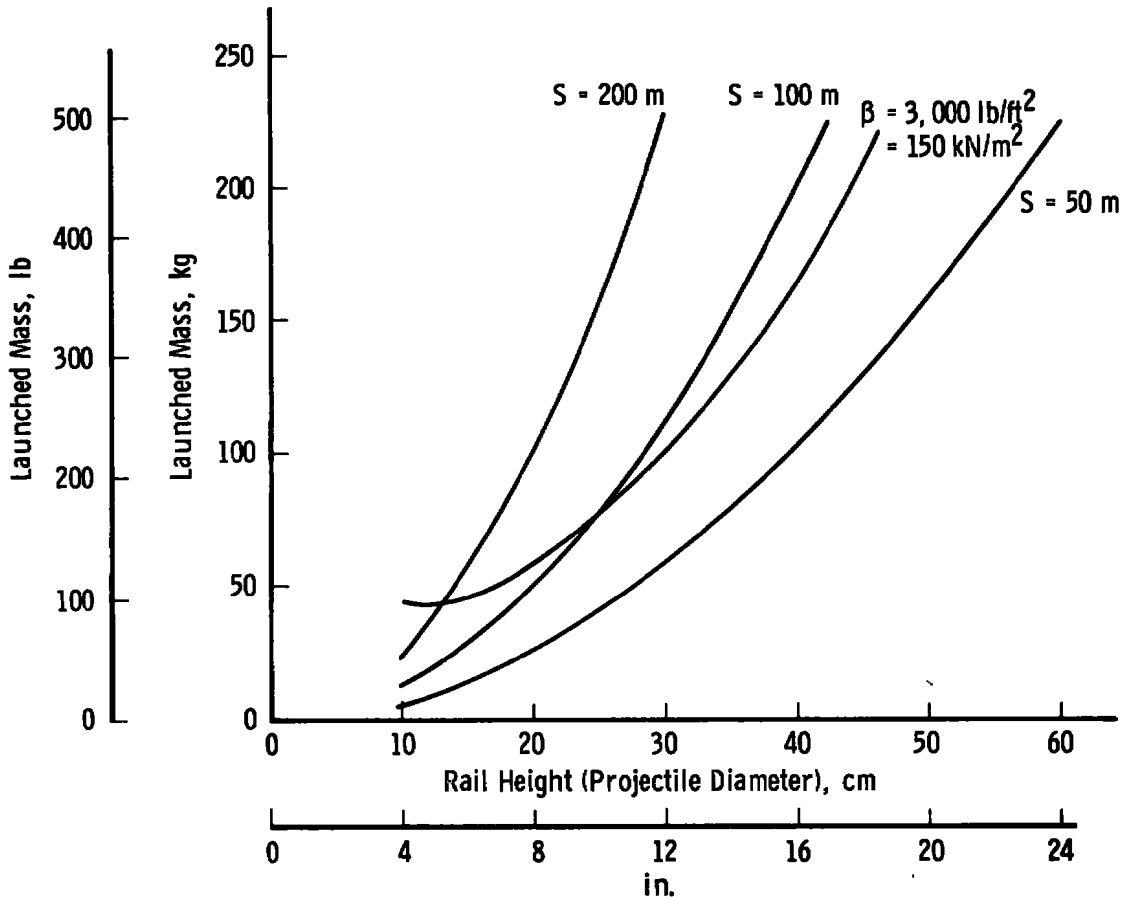


Figure 11. Maximum launchable mass versus rail height.

From Fig. 11 it is apparent that to obtain a $\beta = 150 \text{ kN/m}^2$ the required gun length is somewhat dependent on the desired projectile diameter. It must be noted that longer guns produce lower accelerations, but wear and losses would be expected to rise. The average acceleration required to reach 6 km/sec is indicated in Fig. 12. As we shall see later, acceleration constancy must be traded off against power supply size. The trade off between peak acceleration, stored energy, and gun length suggests a gun length of 200 m with a maximum acceleration ratio of 0.5 (and peak acceleration of $\sim 200,000 \text{ m/sec}^2$). Therefore, 200 m appears to be a reasonable gun length to consider.

The required β should therefore be obtainable down to about 15-cm diameter and easily attainable at larger diameters.

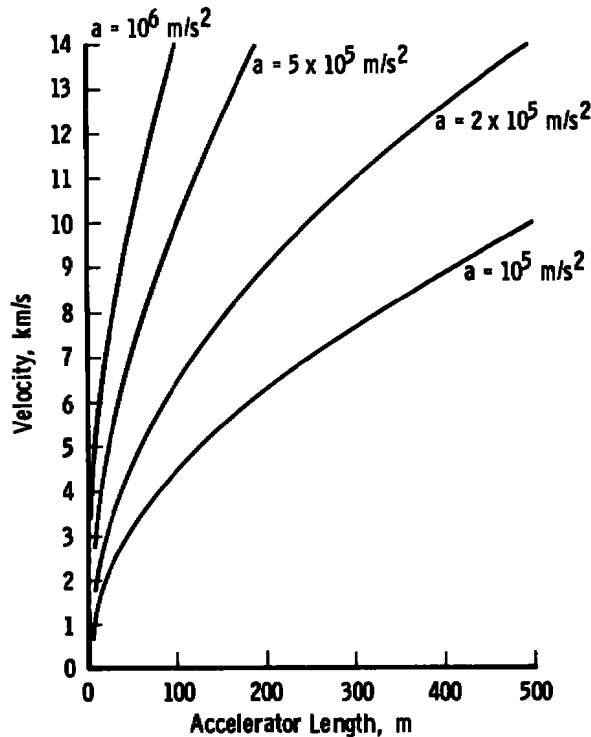


Figure 12. Velocity versus accelerator length.

3.1.3 Electromagnetic Instabilities

At the low acceleration envisioned here, the projectile should behave as a rigid body during acceleration and fluid instabilities should not occur. However, "cocking" may occur and could be prevented by providing sufficient length-to-diameter ratio for the projectile. This could be achieved by spacing out the current-carrying conductors, with spacer material, thus making the projectile effectively longer than "d" (Fig. 2).

The vertical instability, in which the projectile tends to move out from between the rails, will also be present and would require "boxing" in the rails with insulation material. Vertical motion would then be prevented by mechanical restraint.

3.1.4 Contact Phenomena

3.1.4.1 Electrical Behavior

Basically, very low contact resistance is the main electrical requirement. The contact resistance was derived as

$$R = \frac{\zeta}{2} (\pi \sigma / P_n)^{1/2} \quad (2.6)$$

Firstly, this indicates the type of material which makes good contacts - low resistivity and low strength. Copper would be a suitable choice.

Secondly, the normal load-contact number product must be high. As will be seen later, normal load increases friction and wear, so the number of contacts should be large. This may be achieved by making the projectile up of individual leaves with independent fingers on each leaf. In the area available ($\geq 30 \text{ cm}^2$) it should be possible to obtain several thousand individual contact fingers.

The nominal current density (maximum) may be obtained from the resistive heating relation:

$$\int I^2 dt = g_1 A^2$$

or

$$\begin{aligned} (I/A)_{\text{avg}} &= \sqrt{g_1/t} \\ &= \sqrt{\frac{g_1 v}{2x_L}} \quad (\text{constant acceleration}) \end{aligned}$$

Using $v = 6 \times 10^3 \text{ m/sec}$, $x_L = 200 \text{ m}$, and $g_1 = 6 \times 10^{16} \text{ A}^2 - \text{sec/m}^4$

$$\begin{aligned} (I/A)_{\text{avg}} &= 10^9 \text{ A/m}^2 \\ &= 10^5 \text{ A/cm}^2 \end{aligned}$$

Barber (Ref. 5) has reported carrying current densities of up to $\sim 7 \times 10^5 \text{ A/cm}^2$ (203 kA for a 2-g projectile) successfully at a velocity of $\sim 1 \text{ km/sec}$.

In an area of 1 cm^2 it should be possible to obtain at least 100 individual contacts (1 mm square) so the average current per contact I/n should be about 1,000 A.

Barber (Ref. 5) has successfully operated this type of contact up to 1 km/sec, but above this speed transition to arcing was reported. The phenomena is not understood so it is difficult to extrapolate to 6 km/sec, even though the present application is considerably derated from that reported by Barber.

An estimate of the electrical wear of the contact is derived in Section 2.4.3 and the results are depicted in Fig. 8. For a 20-cm-diam (8 in.) launcher 200 m long, the wear would be on the order of 2.5 percent on each side if "good" electrical contact is achieved (0.5 V). Sufficient flexibility and adequate extra material could be built into a projectile to accommodate wear of this magnitude. However, if the contact arcs (~ 10 -V characteristic) the electrical wear becomes catastrophic and successful acceleration appears unlikely.

3.1.4.2 Mechanical Behavior

The frictional force is determined by the normal force and the coefficient of friction. Coefficients of friction have not been measured above about 700 m/sec, and theoretical predictions are varied and unreliable.

The minimum normal force on the contact is that force required to obtain a large enough metal-to-metal contact to keep the contact voltage below 0.5 V or so. Wear due to friction is related to the normal load and the coefficient of friction. The calculations are carried out in Section 2.4.3 and the results are shown in Fig. 9. The worst case is for a mass of 200 kg (40-cm diameter) where, for $\mu_f = 0.2$, approximately 2 cm of wear (5 percent) results. This could probably be accommodated with suitable projectile construction, but for $\mu_f = 0.5$, wear is 10 percent and this would probably be difficult to cope with.

Friction also represents an energy loss to the system and reduces the force available for acceleration. If the energy dissipated in friction is even a fraction of the total kinetic energy, the entire projectile would probably be melted. The kinetic energy at 6 km/sec is $\sim 18 \text{ MJ/kg}$ while the energy required to melt copper is $\sim 400 \text{ kJ/kg}$; therefore, the ratio of friction to acceleration forces must be much less than 0.02 or the projectile will be completely melted.

3.1.5 Driving Method and Energy Storage

Because of model fragility it is advisable to keep the peak acceleration, during launch, relatively low (say less than $200,000 \text{ m/sec}^2$). As the average (constant) acceleration required to reach 6 km/sec in 200 m is $90,000 \text{ m/sec}^2$, this implies an acceleration ratio ($\gamma = a_{\text{avg}}/a_{\text{max}}$) of 0.45 or greater. To achieve acceleration ratios in this range, inductive driving appears to be more appropriate than capacitor driving. As an added advantage, inductive energy storage at the large energies envisioned here is considerably less costly than capacitive storage (Ref. 13).

The calculations in Section 2.5.2 indicate that, for inductive drive, there is a direct trade off between energy efficiency (and thus cost) and acceleration ratio (Fig. 10). That is, high acceleration ratios imply low energy efficiency, high stored energy, and high cost. As these calculations were made neglecting losses (both resistive and mechanical), further calculations were carried out on a digital computer to evaluate the effect of resistive losses. (Mechanical and aerodynamic losses must be negligibly small to prevent projectile melting during acceleration.) The results for a typical gun are shown in Fig. 13. The trade off between efficiency (cost) and acceleration ratio are shown in Fig. 14, for both the lossless case and including resistive losses. Resistive losses make the trade off less attractive at low acceleration ratios. From Figs. 13 and 14, and recalling that the acceleration ratio should be 0.45 or better to ensure adequately low peak acceleration, it appears that a suitable operating point might be at $L_0/L'x_L = 1$ with $\gamma = 0.47$ and $\eta = 0.36$. The energy stored in the driving inductance must then be ~ 2.8 times the final kinetic energy of the projectile.

The inductance per unit length L' is fixed at $0.6 \mu\text{H/m}$ by the geometry of the projectile, and the gun length x_L is fixed at 200 m by ballistic coefficient and acceleration considerations. The value of the required storage inductance can readily be calculated and is $L_0 = L'x = 120 \mu\text{H}$. The energy and inductance may then be used to calculate the initial current required.

Using $\beta = 150 \text{ kN/m}^2$ ($3,000 \text{ lb/ft}^2$) the stored energy required as a function of projectile diameter is shown in Fig. 15 [$E_{\text{store}} = (mv^2)/(2\eta)$].

The inductively stored energy must be supplied from some primary source which might be a rectifier system or a rotating machine

(homo or uni polar generator). A homopolar generator is probably the most feasible for the energies envisioned here.

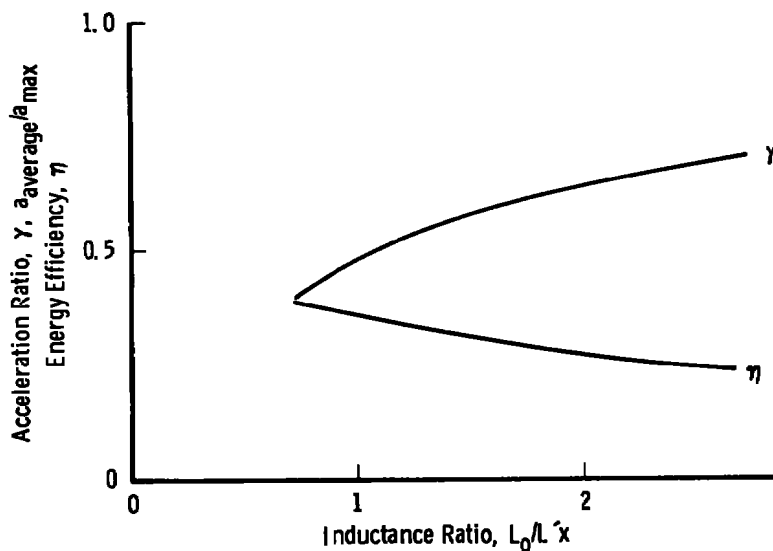


Figure 13. Efficiency and acceleration ratio versus $L_0/L'x$.

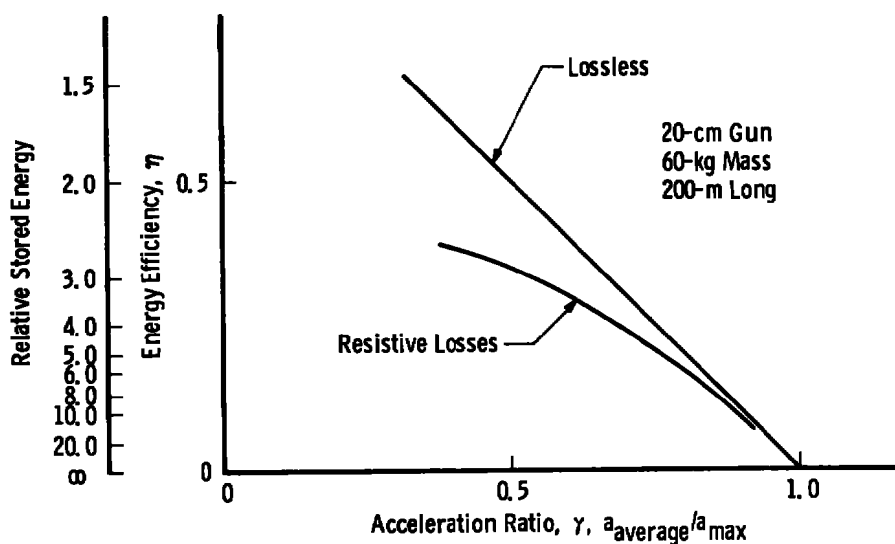


Figure 14. Efficiency versus acceleration ratio.

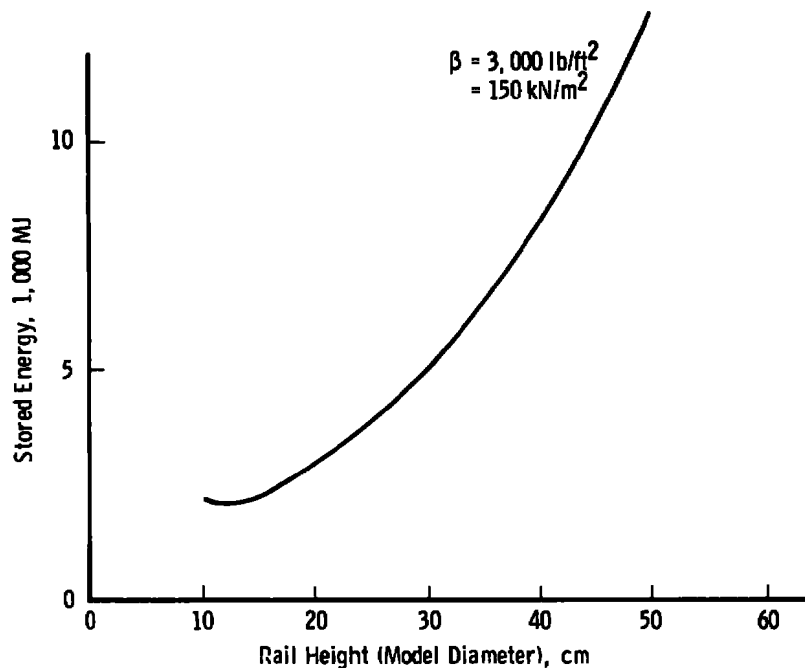


Figure 15. Stored energy versus projectile diameter.

Transfer of energy from the primary store (H. P. G.) to the secondary or driving store (inductor) will also involve energy losses, so the total energy of the system must be greater than indicated in Fig. 15. The efficiency of the transfer will be related to the time constant of the inductance (L_O/R_O) and the voltage of the supply (i. e., the time taken to charge the inductance). Increasing L_O/R_O and increasing voltage both increase efficiency but also increase the cost of the installation. An optimum efficiency could be found if the relative costs of increasing voltage and L_O/R_O were known. An efficiency of 0.5 is probably achievable and will be used in further consideration.

Switching of the currents and energies into the various devices could raise some problems but the experience at the Australian National University (Ref. 12) indicates that they could be overcome.

3.1.6 Possible Configurations and Costs for Launchers

From the considerations in the preceding sections, a number of aspects of the specific configuration of various elements of the launcher system emerge. The launcher system will be divided into: the gun, the launch package, and the power supply, each treated separately.

3.1.6.1 Gun

The gun includes only the rails and supporting structures.

The rail height and rail gap width are equal to the model diameter as this provides the smallest projectile. The geometry of the rail system is square (height = gap) independent of size. (If necessary, a curved rail section could be employed to accommodate an axially symmetric projectile and, providing the geometry remained essentially square, the performance would be the same as for the rectangular rail system considered here).

If the rail thickness is less than the skin depth, the rail thickness controls the electrical resistance of the gun and thus the resistive losses during launch. As rail thickness is increased, losses drop until the rail thickness is equal to the skin depth. Further increases in rail thickness have no further effect on losses as current never flows in the added material. Therefore, the optimum rail thickness is equal to the skin depth. The skin depth is given by $\sqrt{\pi \xi t / \mu_0}$ and the acceleration time, from gun simulations, is about 55 m/sec, so for copper rails the optimum thickness is about 5 cm (2 in.) and this is independent of projectile size.

The rails experience a "magnetic pressure" forcing them apart and suitable restraining structures must be provided. The magnetic pressure P_m is given by

$$P_m = B^2 / 2\mu_0$$

where B is the magnetic field at the rail surface and may be calculated from

$$B = \mu_0 I / h$$

I/h is a maximum for 20-cm-diam guns and falls slightly (for constant β models) with increasing diameter. The maximum magnetic pressure will therefore be experienced on 20-cm guns at maximum β . The simulations indicate that a maximum current of about 6 MA is required. The corresponding pressure is

$$P_m = 5.67 \times 10^8 \text{ N/m}^2 (82 \times 10^3 \text{ psi})$$

A schematic restraining structure is shown in Fig. 16. This is not meant to be a serious design, but simply an aid to estimating materials and cost.

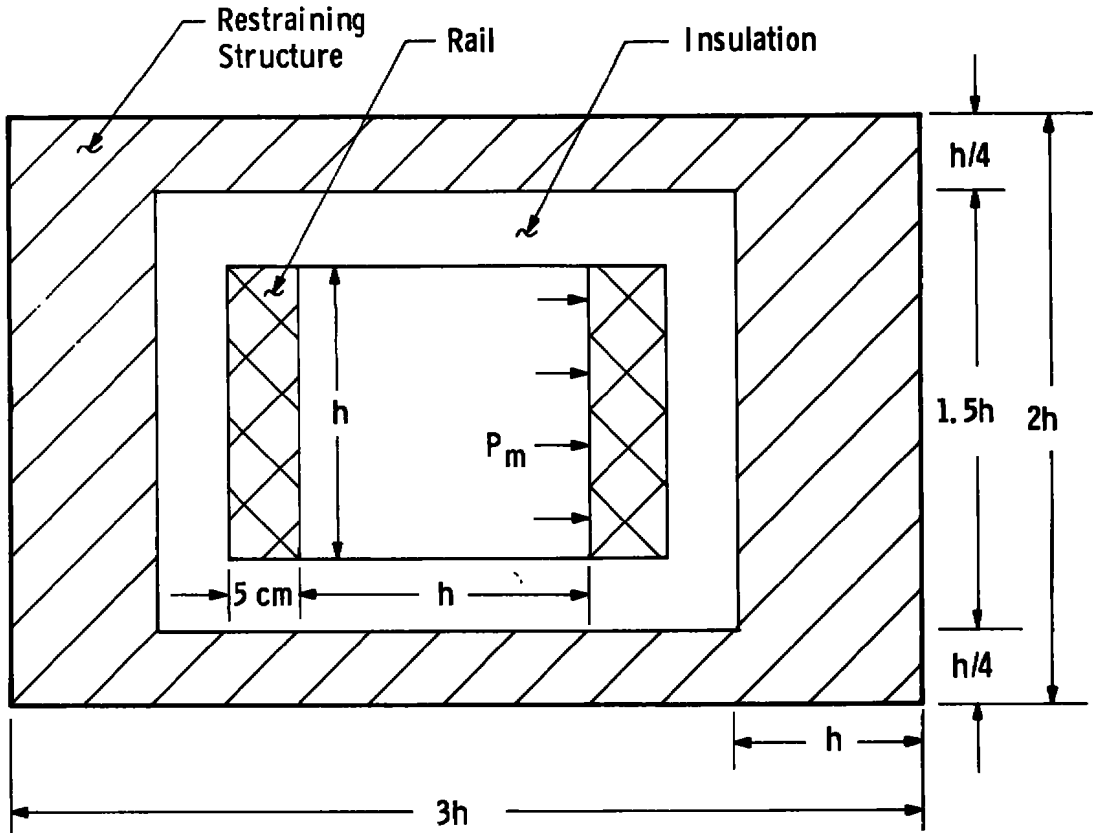


Figure 16. Rail gun restraining structure.

The restraining structure absorbs the magnetic pressure load on the rails in tension. If the restraining material is twice as strong as the maximum magnetic pressure, then only one-half the rail height of material is needed as shown in Fig. 16. Other dimensions are simply assumed as "reasonable." The volume of restraining material required is then

$$\begin{aligned} V_{\text{restrain}} &= 2(3h \times h/4) - 2(3/2)h \times h \\ &= (3/2)h^2 + 3h^2 = (9/2)h^2/\text{unit length} \end{aligned}$$

The volume of rail material required is

$$V_{\text{rail}} = t_{\text{rail}} h/\text{unit length}$$

where t_{rail} is the rail thickness (fixed). If the cost may be represented as proportional to the volume (or mass) of material, then the cost of the gun will be

$$C_{\text{gun}} = (K_{\text{restrain}} \times V_{\text{restrain}} + K_{\text{rail}} \times V_{\text{rail}})$$

If the rails are copper and estimating the installed cost of the copper rails at $90 \times 10^3 \text{ } \$/\text{m}^3$ ($\sim \$5/\text{lb}$) and a steel restraining structure at $70 \times 10^3 \text{ } \$/\text{m}^3$ ($\sim \$5/\text{lb}$), then the cost becomes

$$C_{\text{gun}} = 0.9h + 63h^2 \text{ (M\$)(h in meters)}$$

This is plotted in Fig. 17. It should be noted that the rail cost is only a small proportion of the gun cost (less than 10 percent for the range of h of interest).

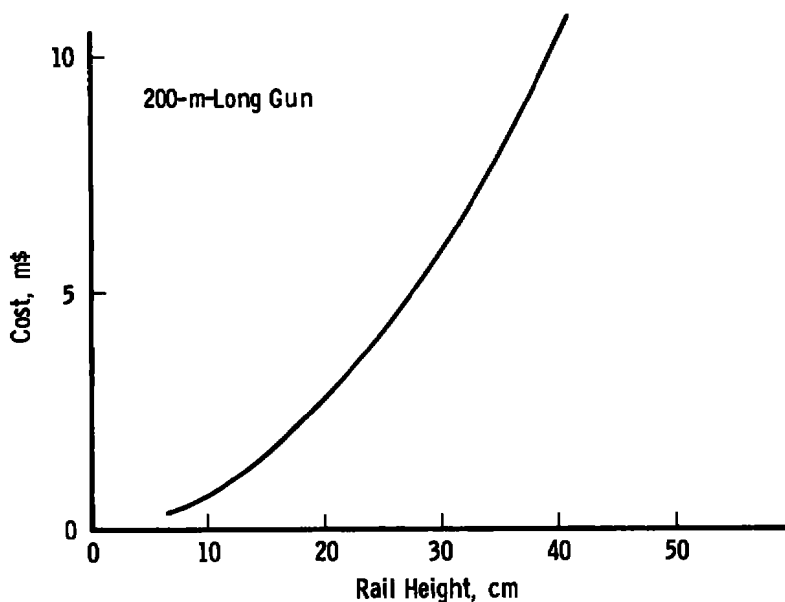


Figure 17. Estimated gun cost versus size.

3.1.6.2 Projectile

The launch package is made up of the projectile plus the model. This section is primarily concerned with the projectile or driving part of the launch package.

A schematic representation of a possible geometry is shown in Figs. 18 and 19. The main features of the suggested construction are:

1. The laminated sections contain sufficient copper to provide adequate current-carrying cross-sectional area plus perhaps some extra.
2. The edges of the leaves are slit into fingers as shown to provide approximately 100 fingers/cm² of cross-sectional area.
3. The trailing edges of the leaves are swept back at an angle to provide flexibility at the contacts to obtain the required normal forces against the rail by redirecting a fraction of the acceleration force, and to accommodate wear while maintaining electrical contact.
4. Spacers between the leaves ensure that the trailing edges do not interfere and that all leaves touch the rail.
5. The spacer block provides adequate length to prevent "cocking" in the gun and brings the package weight up to the required value to obtain the desired ballistic coefficient.
6. The test article is attached to the front of the projectile. This type of construction has been used successfully in the Australian National University (ANU) rail gun (Refs. 5 and 12). The leaves could be conveniently mass produced and possibly reusable. The cost of a projectile would depend largely on the mass of copper used.

A variety of projectile constructions might be considered and a final choice would probably be determined by contact considerations. More sophisticated leaf constructions such as depicted in Fig. 20, might be necessary to overcome contact difficulties. Projectile design and cost therefore rest largely on the successful solution of high-speed contact problems.

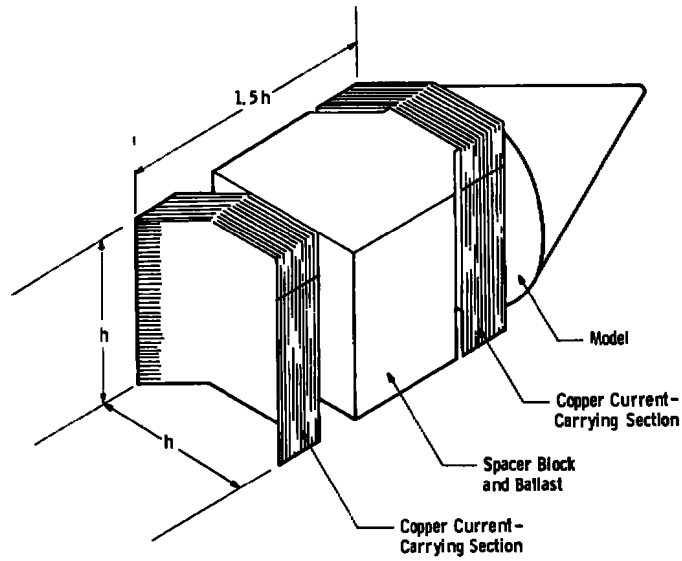


Figure 18. Possible launch package geometry.

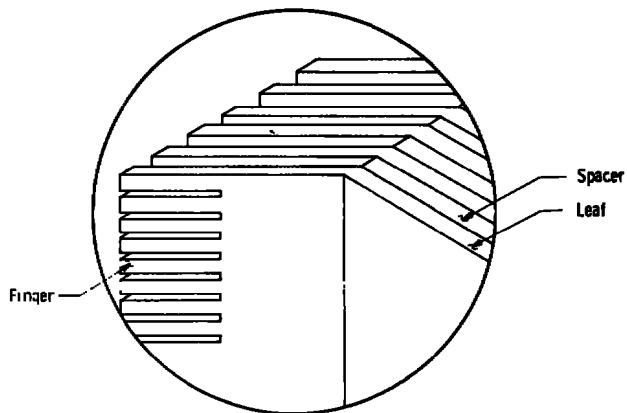


Figure 19. Projectile contact detail.

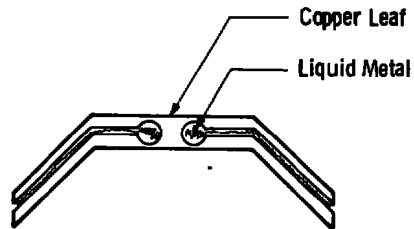


Figure 20. Possible improved contact leaf.

3.1.6.3 Power Supply

The power supply configuration that has emerged consists of a homopolar generator primary supply and an inductive intermediate storage. The inductive store is charged by the homopolar generator and then discharged into the rail gun.

The inductor could be a simple solenoid. The required value of $120 \mu\text{H}$ would not be difficult to obtain in a reasonable sized coil. It would have to be capable of carrying the required acceleration current which depends on the mass being accelerated and varies from $\sim 6 \text{ MA}$ for 50 kg to $\sim 12 \text{ MA}$ for 200 kg . The maximum energy stored in the inductor as a function of projectile size is shown in Fig. 15.

The homopolar generator primary supply must store enough energy and current to charge the inductor. In general, the efficiency of the homopolar generator to inductor transfer will be less than 1. An estimate of cost versus deliverable (i.e., inductive) energy for such a system is shown in Fig. 7 of Ref. 13. Extrapolating to the ranges of interest here ($10^9 - 10^{10} \text{ J}$), we see that the unit cost is ~ 1 to 2 cents/Joule . Applying this unit cost range to the energy storage requirements indicated in Fig. 15 gives the cost versus projectile size.

Comparison with Fig. 17 indicates that the cost of the gun itself will be only a small fraction of the power supply cost.

3.2 SUSTAINER

3.2.1 Introduction

The drag force on a reentry vehicle is characterized by the ballistics coefficient (β) of the vehicle

$$\beta = mg/C_D A_r$$

where m is the mass, C_D the drag coefficient, A_r the aerodynamic cross-sectional area, and g is the acceleration of gravity. The drag deceleration may then be written as

$$a = \rho v^2 g/\beta \quad (3.1)$$

where ρ and v are the free-stream density and velocity. Vehicles of the same ballistic coefficient therefore experience the same drag deceleration.

This report is concerned with vehicles reentering the earth's atmosphere, so the free-stream density as a function of altitude is known. A reentry velocity of 6 km/sec has been chosen and computer calculations made of the reentry trajectories for vehicles with ballistic coefficients of interest (40 kN/m² to 150 kN/m²).

It is found that forces, accelerations, heating and ablation are important for only the last ten seconds of flight (60 km). The relative velocity over the last 60 km of flight is shown in Fig. 21. It is apparent that vehicles of lower ballistic coefficient undergo greater deceleration.

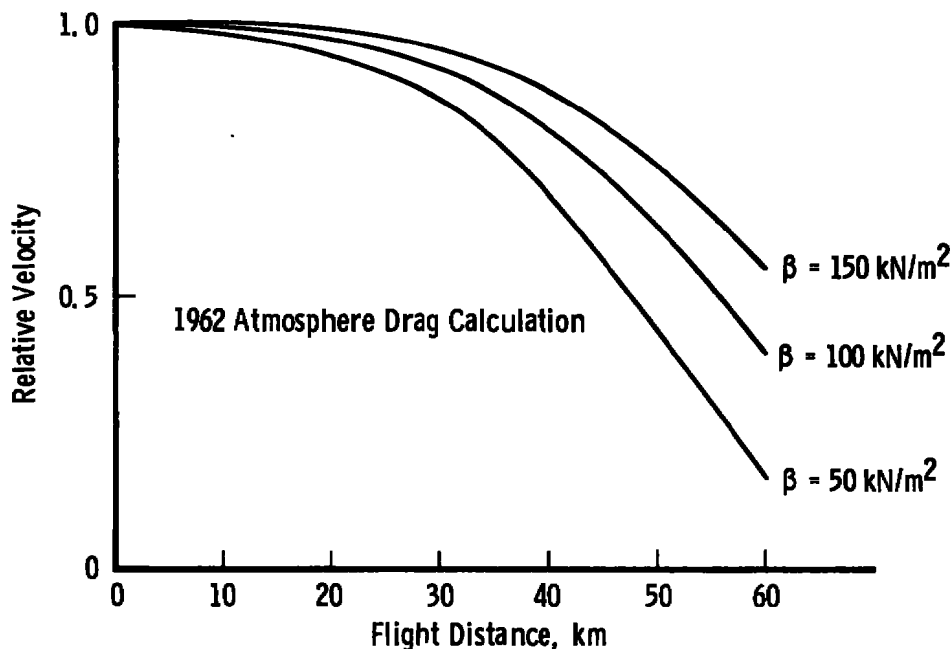


Figure 21. Relative velocity versus flight distance.

Drag deceleration dissipates some of the kinetic energy of the vehicle; this dissipated energy is responsible for the heating and ablation of the vehicle and is of primary interest in the simulation of reentry vehicles. The relative dissipated energy for the final 60 km of flight is displayed in Fig. 22. The slope of these curves at any point is proportional to the deceleration force at that point and it is of

interest that the maximum slope is approximately equal to the total energy dissipated divided by 30 km and is almost independent of ballistic coefficient for the ranges of interest here.

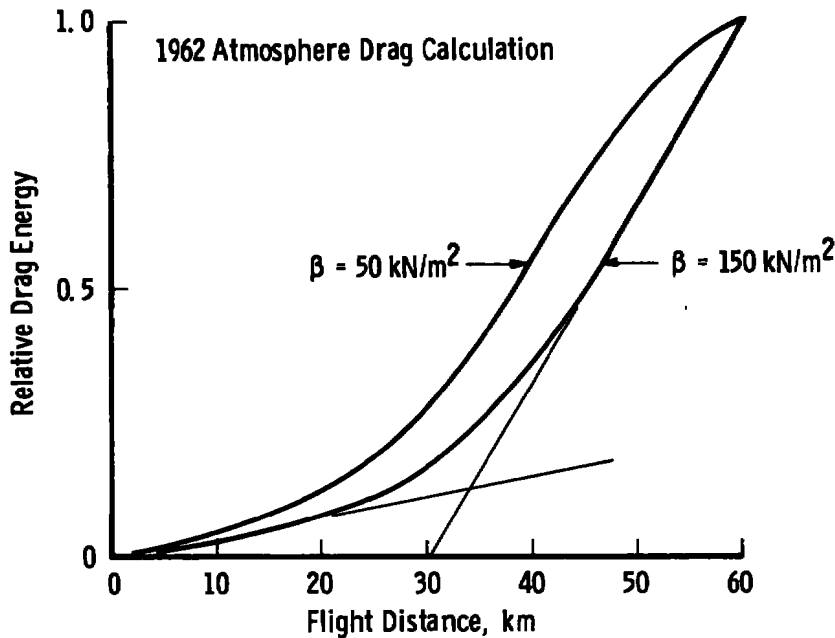


Figure 22. Relative sustaining energy versus flight distance.

Vehicles of high ballistic coefficient (say 150 kN/m^2) are of most interest; however, models of high ballistic coefficient are difficult to launch. The problem in a test facility is to simulate high ballistic coefficient vehicles with lower ballistic coefficient models. One method of doing this is velocity sustaining, that is, energy is added to the launch package during flight so that the velocity-distance trajectory approximates that of the higher desired ballistic coefficient vehicle. This section of the report will examine rail gun velocity sustaining for models launched from a two-stage gas gun.

3.2.2 Sustaining Forces and Energies

We shall assume for the purposes of this section of the report that models will be launched by a two-stage gas gun and that the models of interest are principally those with $\beta = 150 \text{ kN/m}^2$ and $\theta_c = 10 \text{ deg}$.

The drag energy dissipated during test may be written as

$$\begin{aligned}
 E_d &= \int F_d dx \\
 &= 1/2 m(v_o^2 - v_f^2) \\
 &= 1/2 m v_o^2 (1 - v_f^2/v_o^2)
 \end{aligned}
 \tag{3.2}$$

where F_d is the drag force, m the vehicle mass, v_o the initial velocity, and v_f the final velocity.

The dissipated drag energy is therefore a function of the initial kinetic energy $(1/2)mv_o^2$ and a constant factor, the energy loss ratio $(1 - v_f^2/v_o^2)$. The energy loss ratio is a function of the ballistic coefficient as indicated in Fig. 23 (which is derived from computer calculations of reentry values of v_o and v_f). At low ballistic coefficients the ratio approaches one, that is, all the initial kinetic energy is dissipated.

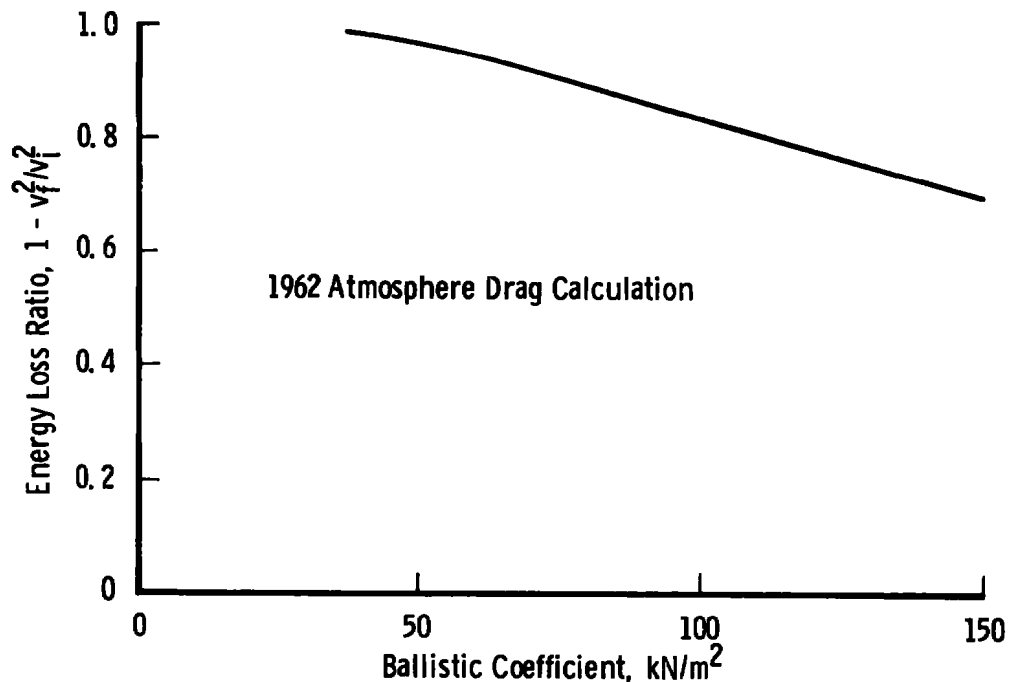


Figure 23. Drag energy loss ratio versus ballistic coefficient.

From Eq. (3.1) it is noticed that the drag deceleration is $a \propto F_d/\beta$, so for a model with desired ballistic coefficient β_D , the desired deceleration is $a_D \propto F_d/\beta_D$. For a model of the same size and shape (i. e., same F_d) but lower ballistic coefficient (mass) the deceleration will be greater than desired, so a sustaining force F_s must be added to produce the desired deceleration, that is

$$a_D = a + a_s$$

or

$$F_d/\beta_D = \frac{F_d + F_s}{\beta}$$

from which the added force may be extracted as

$$F_s = -F_d(1 - \beta/\beta_D)$$

The added force is proportional, but opposite in direction, to the drag force. The constant, $(1 - \beta/\beta_D)$, is the sustaining force ratio and is plotted in Fig. 24 as a function of model diameter for models launched from a two-stage gas gun.

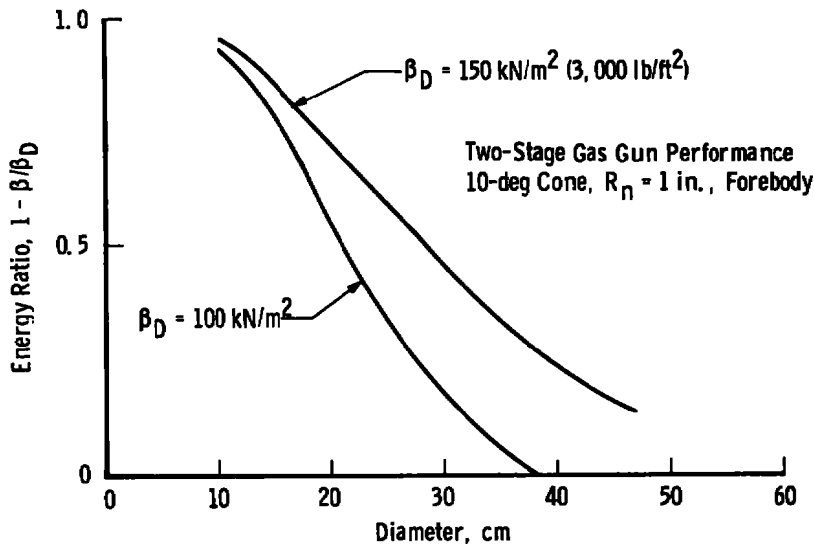


Figure 24. Sustaining energy ratio versus projectile diameter.

The energy that must be added by the sustaining force may be evaluated by integrating the sustaining force

$$\begin{aligned} E_s &= \int F_s dx \\ &= -(1 - \beta/\beta_D) \int F_d dx \end{aligned}$$

The negative sign simply indicates that the energy is added as opposed to $\int F_d dx$ which is dissipated. $\int F \times dx$ from Eq. (3.2) may be expressed as $(1/2) m v_0^2 (1 - v_f^2/v_0^2)$; therefore, the sustaining energy is (neglecting the sign)

$$E_s = (1/2) m v_0^2 (1 - v_f^2/v_0^2) (1 - \beta/\beta_D)$$

which is shown plotted in Fig. 25 for models launched from a two-stage gas gun to 6 km/sec.

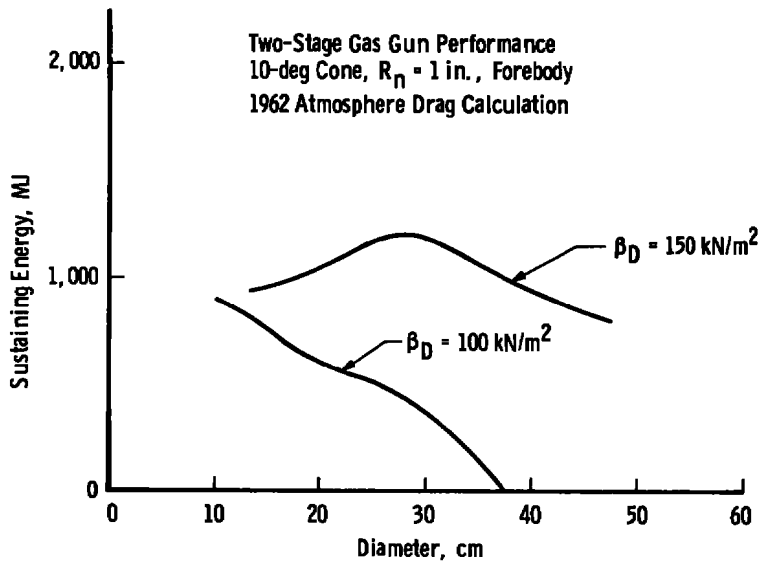


Figure 25. Sustaining energy versus projectile diameter.

The total required sustaining energy as a function of model diameter has now been defined (Fig. 25). However, the manner in which this energy must be added has not. We now consider the sustaining energy and force as functions of flight distance.

The relative sustaining (or drag) force as a function of flight distance is shown in Fig. 26. The curves of different ballistic coefficients

are quite similar in shape which indicates that a sustainer capable of simulating one ballistic coefficient would probably be capable of simulating any ballistic coefficient in the range of interest.

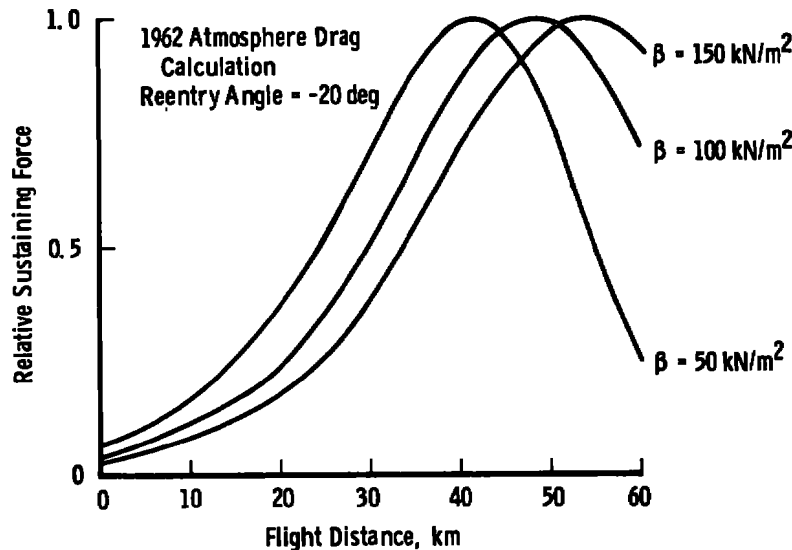


Figure 26. Relative sustaining force versus flight distance.

The relative sustaining energy is directly proportional to the drag energy, so Fig. 22 also represents the relative sustaining energy required as a function of flight distance.

A 60-km range is probably impractical for a number of reasons, so it is necessary to consider the effect on the sustainer of using a shorter range and simulating the complete flight path with a number of shorter flights.

Reducing the range length has no effect on the peak sustaining forces required. Each discrete section of the force-flight distance curve (Fig. 26) must be duplicated as closely as possible. The sustainer should, therefore, be capable of adjustment to obtain any desired section of the curve, both with respect to force magnitude and "shape." Typical required force "profiles" are shown in Fig. 27 for various sections of the flight path.

By reference to Fig. 22 we can evaluate the effect of range length on the maximum sustaining energy that must be supplied. The straight line drawn from the 30-km point to the maximum energy at 60 km emphasizes three points:

1. Very little energy is required in the first half of the flight path and this implies that a range length of between 30 km and 60 km would require virtually the same energy as a 60-km range.
2. Below a range length of 30 km the energy required is almost a linear function of range length as shown in Fig. 28. For example, a range length of 10 km requires only about one-third of the total sustaining energy for a complete reentry simulation.
3. The slope of this line is approximately equal to the maximum sustaining force (i. e., the maximum sustaining force is approximately equal to the total sustaining energy divided by 30 km). Reducing range length therefore reduces the amount of energy required but does not affect the magnitude of the forces required. In addition, reduced range length requires that the sustainer be flexible, that is, capable of variation in force, magnitude, and shape. The ability of a rail gun to meet these criteria will now be examined.

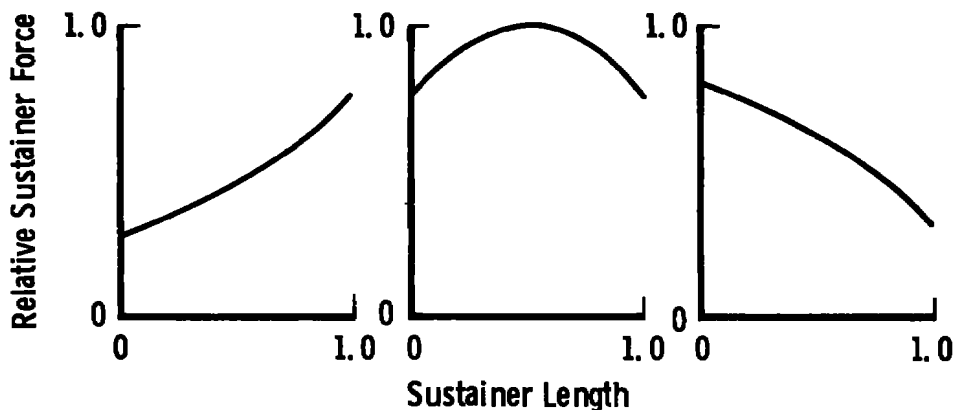


Figure 27. Sustaining force profiles for reentry simulation.

3.2.3 Rail Gun Sustaining Operational Limitations

3.2.3.1 Rail-Projectile Geometry

The projectile considered here will be launched from a two-stage gas gun and would most probably be axially symmetric. The sustainer rails would, therefore, have to be axially symmetric also. Because of

possible unwanted aerodynamic interactions between the model and the rails, it would be desirable to have an "open" rail system which would allow gas to flow as unimpeded as possible around the model. The rails must have adequate current-carrying capacity and contact area to pass the required sustaining current. The geometry chosen for this study is depicted in Fig. 28. This geometry may not be the only possible one or the optimum, but is representative of what might be employed.

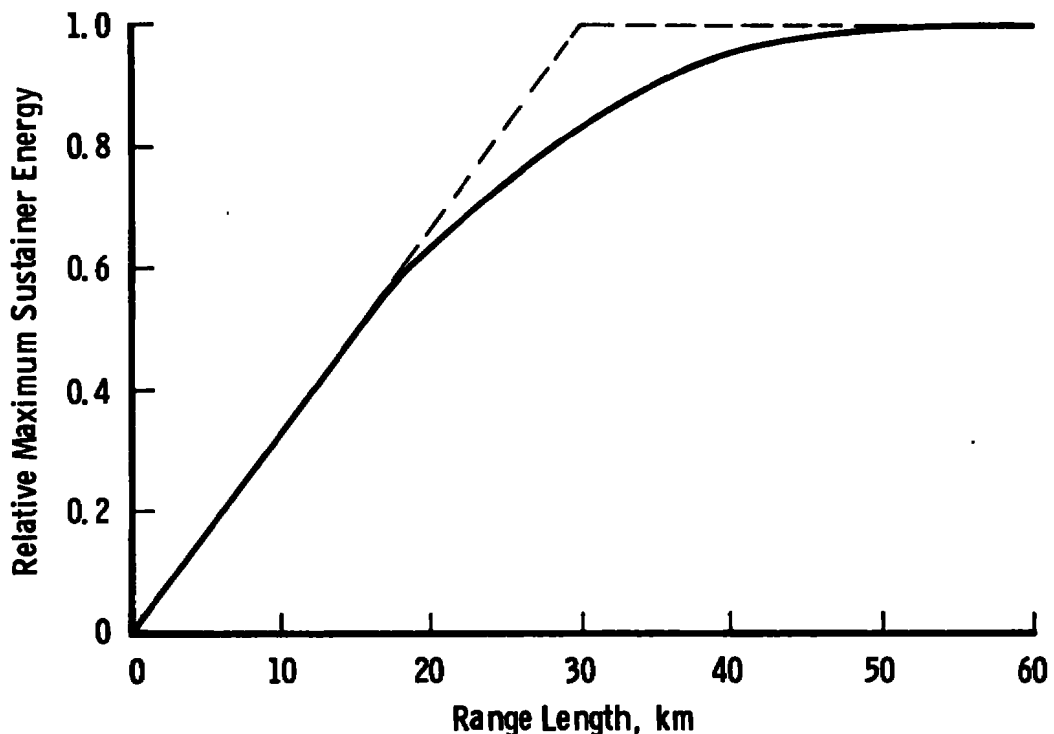


Figure 28. Relative maximum sustaining energy versus range length.

The rails in Fig. 29 may be considered as two separate rail pair systems rotated at 90 deg to each other. As they are at 90 deg to each other, they are decoupled and may be considered as two separate rail systems in parallel. The effective inductance per unit length of the rails is therefore one-half the inductance per unit length of one opposing pair of rails. The inductance per unit length of one pair of rails is a function of the ratio of model diameter to rail height (D/h). Providing h is small compared to D , the inductance is approximated by the parallel plate case in which the inductance is a function of (w/h). Results for the parallel plate case are shown in Fig. 3.

Choosing $D/h \sim 4$, L' for one pair of rails is approximately $1.2 \mu\text{H/m}$ and for the complete rail system $L' = 0.6 \mu\text{H/m}$, which is the same as that used for the launcher calculations.

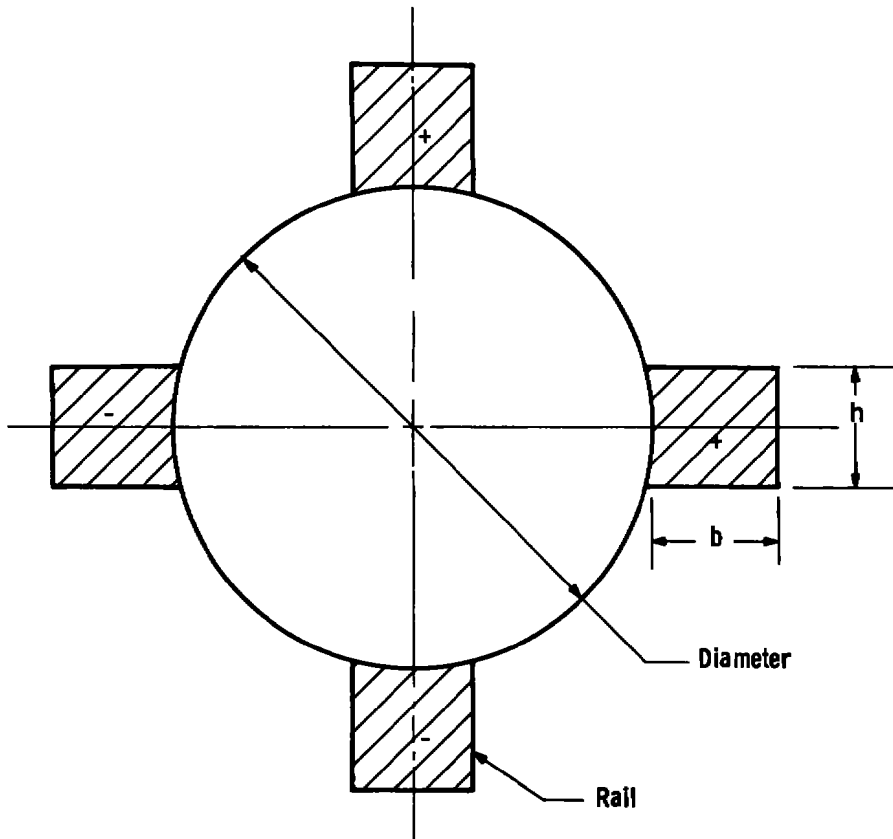


Figure 29. Sustainer rail geometry.

The sustaining force is therefore $F_S = L'I^2/2$ and from this an estimate can be made of the maximum current required. The maximum force is given approximately by the total required sustaining energy divided by 30 km (Section 3.2.2). From Fig. 25 it is apparent that for the worst case the total sustaining energy is about 1,200 MJ. Therefore, the maximum required force is about 40 kN which corresponds to 365 kA of current.

3.2.3.2 Ohmic Heating

Let us consider a range of length ℓ divided into n sustaining sections with sustainers of length s_S . The total range length ℓ may not be completely occupied by sustainer, that is, there may be periods of

free flight following sustaining. If the sustaining to range distance ratio is denoted by γ_s , then

$$\gamma_s = \frac{n s_s}{\ell} \leq 1$$

If a sustaining current of I is passed during sustaining, then the ohmic heating (for each sustainer) may be expressed by the action integral (Section 2.2) as

$$\int I^2 dt = g_1 A^2$$

and for n identical sustainers

$$n \int I^2 dt = g_1 A^2$$

which may be rewritten in terms of the sustaining force $F_s = L' I^2 / 2$ as

$$\frac{2n}{L'} \int F_s dt = g_1 A^2$$

where the $\int dt$ is across one of n identical sustainers.

To facilitate analysis we shall consider the case where the projectile model is at constant velocity (v) in the range, and a constant sustaining force F_s (or some equivalent) is applied throughout the entire flight. These approximations are most valid in the 40- to 60-km range of the flight path (Fig. 26) and as this range is the most difficult to obtain, the following analysis is probably a pessimistic assessment of ohmic heating.

If F_s is the constant required sustaining force, the same energy may be added in n identical sustainers by a force

$$F_{sn} = F_s / \gamma_s$$

where γ_s is the sustaining-to-flight distance ratio. The previous equation may then be written as

$$\frac{2n}{L'} \int \frac{F_s}{\gamma_s} dt = g_1 A^2$$

and noting that F_s is a constant, $t = \ell/v$, and $n/\gamma_s = \ell/s_s$

$$A^2 = \left(\frac{2 F_s \ell}{L' n g_1} \right) \quad (3.3)$$

Now for the geometry of interest here (Fig. 29), the current-carrying cross-sectional area A is

$$A^2 = (2h)^2 d^2$$

or, in terms of the projectile diameter ($D = 4h$)

$$A^2 = \frac{D^2}{2} d^2$$

Now d cannot be arbitrarily large due to the skin effect, that is $d \leq \delta$, where $\delta = \sqrt{\pi \xi t / \mu_0}$, the skin depth for time (t). For the case of copper ($\xi \approx 2 \times 10^{-8} \Omega - m$), $\delta \approx 0.22 t^{1/2}(m)$, and for $d = 0.5 \delta$, $d = 0.11 t^{1/2}$. Therefore,

$$A^2 = \frac{D^2}{4} (1.21 \times 10^{-2} t)$$

which may be substituted into Eq. (3.3) to yield

$$\frac{D^2}{4} (1.21 \times 10^{-2} t) = \frac{2 F_s \ell}{L' v g_1}$$

Noting that $vt = \ell$, the minimum diameter D may be extracted

$$D = \left(\frac{8 F_s}{1.21 \times 10^{-2} L' g_1} \right)^{1/2} \left(\frac{\ell}{s_s} \right)^{1/2} \quad (3.4)$$

As noted in Section 3.2.2 the maximum force F_s is given approximately by $F_s = E_{\text{total}} / (30 \times 10^3)$ where E_{total} is the total sustaining energy that must be supplied. From Fig. 25 it can be seen that the worst case requires about 1,200 MJ of energy or $F_s \approx 40,000$ N. L' is determined by the geometry and is $\approx 0.6 \mu H/m$. We shall take $g_1 \approx 6 \times 10^{16} A^2 - \text{sec}/m^4$ which is equivalent to copper derated about 30 percent from melting. Figure 30 illustrates Eq. (3.4) with the above values of the parameters, and may be interpreted as the minimum diameter that can be sustained for a given sustainer/range

length ratio or the minimum sustainer/range length ratio that may be employed with a given diameter of projectile.

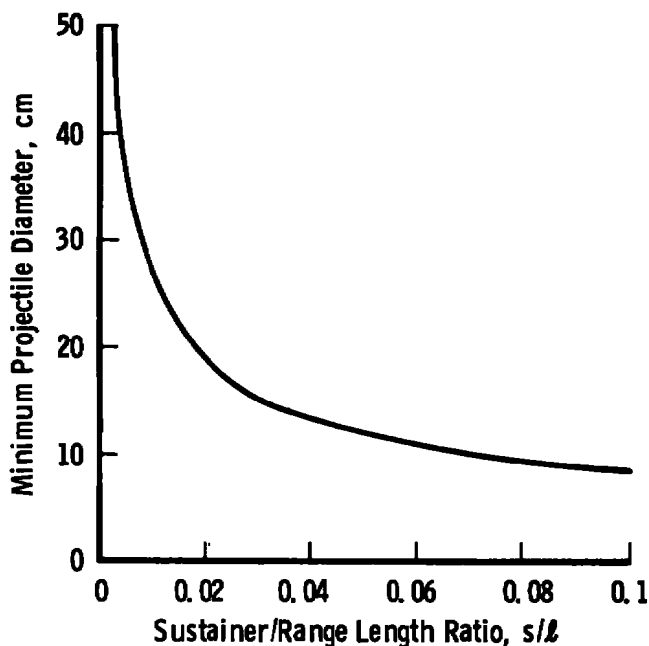


Figure 30. Ohmic heating limitations.

It is apparent from Fig. 30 that sustainer lengths of 0.1 of the range length or greater provide safe operation from an ohmic heating point of view for projectiles of interest here (diameters greater than 10 cm).

3.2.3.3 Electromagnetic Instabilities

Sustaining involves comparatively low accelerations and the projectile can be expected to behave as a rigid body, thus effectively eliminating hydromagnetic instabilities. The rail geometry envisioned (Fig. 29) should provide guidance and could be used to enhance the aerodynamic and electromagnetic stability of the launch package.

3.2.3.4 Contact Phenomena

The contact behavior described in Section 3.1.4 for a launcher might also be expected to occur in a sustainer. However, sustaining differs from launching in three important aspects:

1. Sustaining is required over much longer distances (up to two orders of magnitude longer).
2. Sustaining requires very much lower average currents (at least one order of magnitude lower).
3. Sustaining takes place entirely at high velocity.

These three factors might be expected to reduce the relative importance of electrical effects and increase the importance of mechanical effects. For example, the high velocities and very long sliding distances might be expected to produce appreciable mechanical wear; however, the relatively low electric currents carried might not greatly increase that wear. It might be expected, therefore, that sustainer contact phenomena will be mechanically dominated.

The almost total lack of data on sliding contacts at sustaining velocities makes it very difficult to arrive at any realistic quantitative conclusions and the entire problem remains an important unknown.

3.2.4 Rail Gun Sustainer Driving Methods

3.2.4.1 Sustainer Configuration

It is advantageous at this point to describe in some detail what a range sustainer might consist of and how it might operate.

Basically, the system would consist of a range of some length (ℓ) into which a projectile model of some diameter (D) is launched by a gas gun. The diameter (D), together with the ballistic coefficient that is to be simulated, determines the total sustaining energy that must be supplied to the launch package during a complete reentry simulation (Fig. 25). If the complete reentry is simulated in sections in a range less than 60 km long, the total energy per flight is reduced by a factor which is a function of the range length (Fig. 28). Therefore, launch package diameter, required model ballistic coefficient, and range length determine the amount of energy that the sustainer must supply to the launch package in the range.

The sustainer may be divided up into a number of separate independent rail gun sections within the range with each sustainer section adding a fraction of the total energy. The number of sections that may be employed is limited by ohmic heating effects which limit the sustainer/range length ratio (Fig. 30). The range is therefore divided into

n sections each of which is ℓ/n long and $n \geq 1$. In each section there is a sustainer of length s_s , where the ratio s_s/ℓ is greater than or equal to that depicted in Fig. 30. The extremes of configuration that might be realized are as follows:

1. $n \equiv 1$, $s_s = \ell$; that is, there is one sustainer section and the sustainer is the same length as the range.
2. $n \equiv 1$, $s_s/\ell = \text{limit}$; there is one sustainer section but the sustainer does not extend for the entire range length; it is as short as ohmic heating will permit. This shortened sustainer must supply the same total energy to the launch package as that in No. 1 above, therefore, the peak and average sustaining forces must be much higher.
3. $n \equiv \ell/s_s$, $s_s/\ell = \text{limit}$; that is, the sustainers are as short as ohmic heating will permit and they are arranged "end to end" to cover the entire range.

Any arrangement within these extremes may, of course, be employed.

The advantages and disadvantages of each of the extreme cases considered above are as follows:

1. $n \equiv 1$, $s_s = \ell$. This arrangement provides the "smoothest" acceleration. However, the required force "shape" is difficult to obtain, and the velocity profile is therefore not exactly as desired. Resistive losses in the sustainer rails seriously degrade the energy efficiency of the sustainer as s increases, so energy becomes relatively costly in this case (see following).
2. $n \equiv 1$, $s_s = \ell$ limit. This arrangement abandons attempting to achieve the "exact" velocity profile, but adds the correct amount of energy at some pre-determined part of the flight. As the gun is as short as possible, the resistive losses are as low as possible making the energy efficiency high. The high forces generated could have a serious effect on model integrity and stability.

3. $n = \ell / s_s$, $s_s / \ell = \text{limit}$. This is a compromise between the previous two cases. Sustaining is carried out over the entire length, thus lowering the acceleration forces. However, the acceleration is "bumpy" and periodic which may be detrimental to model integrity and stability despite the lower accelerations. The short sustainers would enjoy low resistive losses and high efficiency.

The basic "unit" sustainer, therefore, consists of a power supply and a rail gun of length s . A number of these "unit" sustainers may be arranged to provide a range of length $\ell \geq s_s$. The two important parameters of these sustainer units which must be evaluated are: (1) force "shape" that can be provided (i. e., force as a function of sustainer distance and (2) energy efficiency (and therefore power supply cost). Both of these parameters depend on driving method and gun length.

3.2.4.2 Driving Methods and Performance

The two basic energy storage methods available for rail gun driving are inductive storage and capacitive storage as discussed in Section 2.5.

Inductive storage has two serious disadvantages for sustainer use as follows:

1. The force varies approximately as $1/x^2$ where x is the distance travelled from the breech. For the very long accelerators required in sustaining, this results in a continuously falling force which does not realistically fit most parts of the sustaining force profile (Figs. 26 and 27). Resistive losses exaggerate this difficulty.
2. The projectile enters the rail gun at high velocity making the necessary accurate timing and rapid switching of the stored current difficult. In order to switch high currents out of inductive storage successfully, very low initial load inductance is required. As the projectile in this case is moving at high velocity, the rail gun inductance increases rapidly and after even a short time ($\sim 10 \mu\text{sec}$) may be too high to switch large current into the sustainer successfully. In any case, the required switch gear would have to be fast, sophisticated, and undoubtedly expensive.

Capacitive storage appears to be more suitable for sustainer driving for the following reasons:

1. The force varies approximately as $1/v^2$ (Section 2.5) and as in the sustainer the velocity v is falling the force could, neglecting losses, actually rise as the projectile proceeds down the sustainer. This would fit at least the major part of the force curve (Figs. 26 and 27) satisfactorily if not exactly.
2. Switching would occur automatically with no additional devices immediately as the projectile enters the sustaining section. The capacitor would be simply charged to the required voltage and connected across the rails. As the projectile enters the sustainer it would complete the circuit and current would begin to flow. The magnitude of the sustaining force could be easily adjusted by adjusting the voltage on the capacitor.

Further consideration will, therefore, be restricted to capacitive energy storage and driving.

The circuit of a capacitively driven sustainer is depicted in Fig. 31 and the equations which describe its operation are as follows:

1. Conservation of energy

$$(1/2)CV_o^2 = (1/2)CV^2 + (1/2)mv^2 + (1/2)(L_o + L'x)I^2 + \int I^2(R_o + R'x)dt + \int F_d v dt$$

2. Voltage around the circuit

$$V_o = \frac{1}{C} \int I dt + I(R_o + R'x) + \frac{d}{dt} (L_o + L'x)I$$

3. Dynamic relations

$$a = L'I^2/2m - F_d/m \text{ or } F = L'I^2/2$$

$$v = \int a dt + V_o$$

$$x = \int v dt$$

To facilitate analysis and comparison of the results and to more closely simulate the actual velocity profile without the added computational complexity of the true drag term in the acceleration expression,

a constant velocity through the sustainer will be assumed. The added sustaining energy is then $\int F_d dx$. The velocity actually falls during sustaining, but if an appropriate mean constant velocity is chosen the results obtained should be adequately accurate for present purposes. The most difficult section to simulate is the 40- to 50-km region (Fig. 26) as high sustaining forces are coupled with high velocities (i. e., high sustaining powers are required). If the desired sustaining profile can be achieved in this section, then the profiles in other sections can also be simulated. The velocity in this region of reentry is about 5 km/sec, so a constant velocity of 5 km/sec will be used in further analysis.

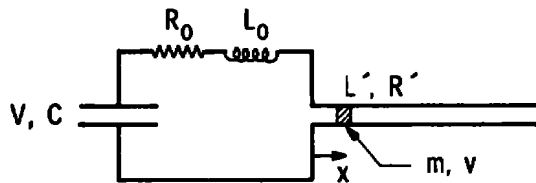


Figure 31. Circuit for capacitively driven sustainer.

If resistive losses are to be considered, the equations describing the behavior of the system must be solved numerically. However, it is informative to find analytic solutions of the "lossless" equations as such a solution yields functional dependences which will enable us to examine the "shape" of the force profile.

The voltage equation (No. 2 above) may be differentiated to yield, neglecting the resistive terms

$$0 = \frac{I}{C} + (L_0 - L'x) \frac{d^2 I}{dt^2} + 2L'v \frac{dI}{dt}$$

where $v = \text{constant}$ and $x = vt$. This may be rearranged to become

$$(a + t) \frac{d^2 I}{dt^2} + \frac{2 dI}{dt} + bI = 0$$

where $a = L_0/L'v$ and $b = 1/(L'vC)$ and the initial conditions are $I(0) = 0$ and $I'(0) = V_0/L_0$. This equation may be transformed by setting $y = a + t$ to yield

$$\frac{y d^2 I}{dy^2} + \frac{2 dI}{dy} + bI = 0$$

and $I(a) = 0$, $I'(a) = V_0/L_0$. Now setting $y = p^2$, the equation further transforms to

$$\frac{d^2 I}{dp^2} + \frac{3}{p} \frac{dI}{dp} + 4bI = 0$$

and $I(\sqrt{a}) = 0$, $I'(\sqrt{a}) = 2V_0\sqrt{a}/L_0$. This may be recognized as a form of Bessel's equation, the roots of which are, $p^{-1}J_1(2\sqrt{b}p)$ and $p^{-1}Y_1(2\sqrt{b}p)$. The solution of the equation is therefore

$$I(p) = p^{-1}(A J_1(2\sqrt{b}p) + B Y_1(2\sqrt{b}p))$$

Application of the boundary conditions provides solutions for A and B

$$A = -\frac{V_0}{L_0} a\pi\sqrt{a} Y_1(2\sqrt{ba})$$

$$B = \frac{V_0}{L_0} a\pi\sqrt{a} J_1(2\sqrt{ba})$$

Transforming back to $I(t)$, the solution is

$$I(t) = \frac{V_0 a}{L_0} \pi \sqrt{\frac{a}{a+t}} \left(J_1(2\sqrt{ba}) Y_1(2\sqrt{b(a+t)}) - Y_1(2\sqrt{ba}) J_1(2\sqrt{b(a+t)}) \right) \quad (3.5)$$

If the current (or force) shape is to be independent of the sustainer length it is apparent from this equation that a/t and ba must be independent of the sustainer length, that is,

$$L_0/L'vt = \text{const}$$

and

$$L_0/(L'v)^2 C = \text{const}$$

which together imply that $L_0 = \text{const} \times \text{sustainer length}$, and $C = \text{const} \times \text{sustainer length}$. If these two conditions are met then the "shape" of force profile should be independent of gun length, neglecting resistance, and when resistance is included, the effect of gun length can be readily assessed.

Let us now examine the asymptotic behavior of Eq. (3.5) to determine the bounds of the behavior of the system. Consider the case when the capacitance C is made very large:

$$\begin{aligned}
 b &\rightarrow 0 \\
 J_1\left(2\sqrt{b(a+t)}\right) &\rightarrow \sqrt{b(a+t)} \\
 Y_1\left(2\sqrt{b(a+t)}\right) &\rightarrow -\frac{1}{\pi} \frac{1}{\sqrt{b(a+t)}} \\
 I &\rightarrow \frac{V_o}{L'v} \left(\frac{t}{a+t}\right) \\
 F &\rightarrow \frac{V_o^2}{2L'v^2} \left(\frac{t}{a+t}\right)^2
 \end{aligned} \tag{3.6}$$

As expected, the force and current are independent of b (or C) and this represents the asymptotic early behavior of the system. For self similar shapes (i. e., a/t independent of sustainer length and $L_O = \text{const} \times \text{length}$) values of F for different values of L_O and typical values of V_O , L' and v are plotted in Fig. 32. It is apparent that a large initial inductance ($L_O' = L's$) greatly retards current buildup, while smaller inductances result in rapid current rise.

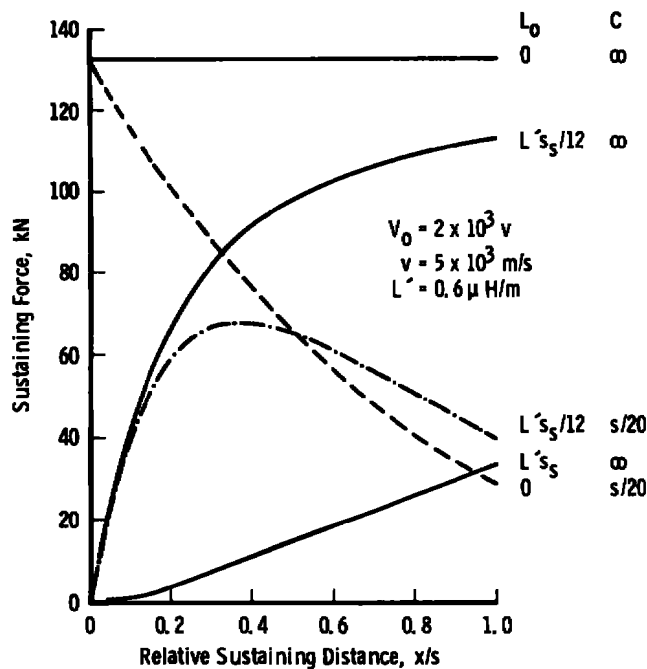


Figure 32. Sustaining forces for capacitively driven sustainer.

The other asymptote of interest is the case where L_0 is zero ($a = 0$) and C is finite (b is finite),

$$a \rightarrow 0$$

$$\begin{aligned} I &\rightarrow \frac{V_o^2}{L'v} \left(\frac{J_1(2\sqrt{bt})}{\sqrt{bt}} \right) \\ F &\rightarrow \frac{V_o^2}{2L'v^2} \left(\frac{J_1(2\sqrt{bt})}{\sqrt{bt}} \right)^2 \end{aligned} \quad (3.7)$$

Equation (3.7) is plotted in Fig. 32 (broken line) and it can be seen that low initial inductance results in a rapid rise of current (to the maximum in zero time) and subsequent sharp current decay. It is apparent that some value of parameters between these extremes is required for an acceptable force shape. Such a choice might be $L_0 = L's_S/12$ and $C = s_S/20$ and Eq. (3.5) is also plotted in Fig. 31 for these values. This value of L_0 yields an acceptable rate of current rise and together with the chosen capacitance provides a relatively flat peak force and slow decay.

Numerical solutions of the equations were found including resistive losses for a 100-m-long sustainer. The effect of varying the storage capacitance C was investigated and the results are shown in Fig. 33. A capacitance of 5F in this figure corresponds to the suggested operating parameter of $C = s_S/20$. It is also noted that this yields a relatively high energy efficiency ($\eta = mv^2/CV_0^2$) of 0.47 combined with a relatively good force profile. The choice of $L_0 = L's_S/12$ and $C = s_S/20$ seems therefore to be an acceptable choice of parameters for the purposes of this study. These are not suggested as the only or optimum parameters that might be chosen, but as a representative choice.

The numerical computer solution of the equations including resistive losses was used to examine the effect on efficiency and force shape of increasing sustainer length. The results are shown in Figs. 34 and 35. Also shown in Fig. 34 is the lossless analytic result. The area under each curve in Fig. 34 represents the useful sustaining energy; therefore, the difference in area between any curve and the lossless curve represents the resistive energy lost. As sustainer length increases, the energy loss increases (efficiency declines) and the shape changes somewhat. The maximum force also declines, but this can be

raised by raising the driving voltage which, in principle, does not affect the efficiency.

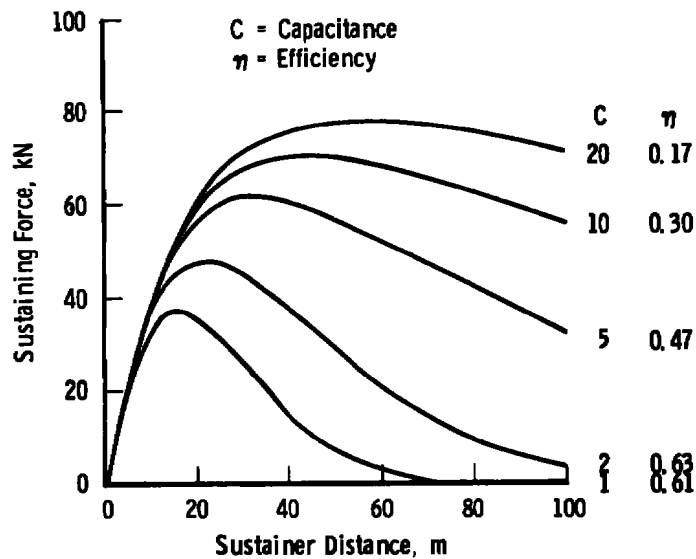


Figure 33. Effect of capacitance on sustaining force.

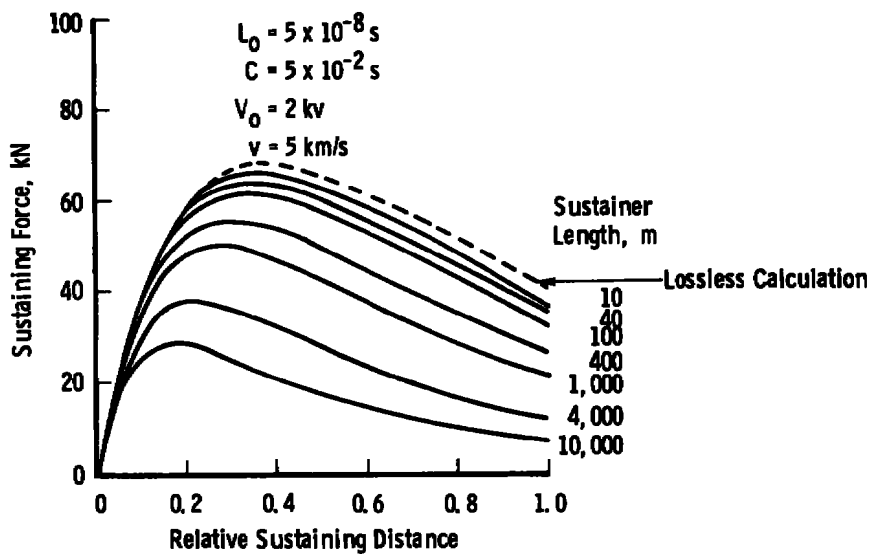


Figure 34. Sustaining force versus relative distance with resistive losses.

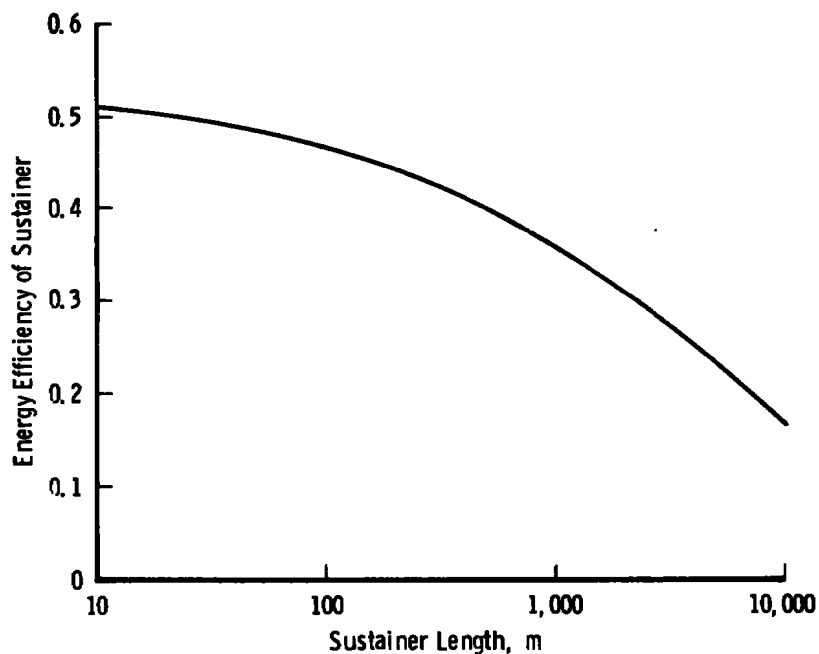


Figure 35. Energy efficiency versus sustainer length.

At long sustainer lengths the shape can be corrected somewhat by increasing the driving capacitance, but the efficiency declines to very low values as shown in Fig. 36.

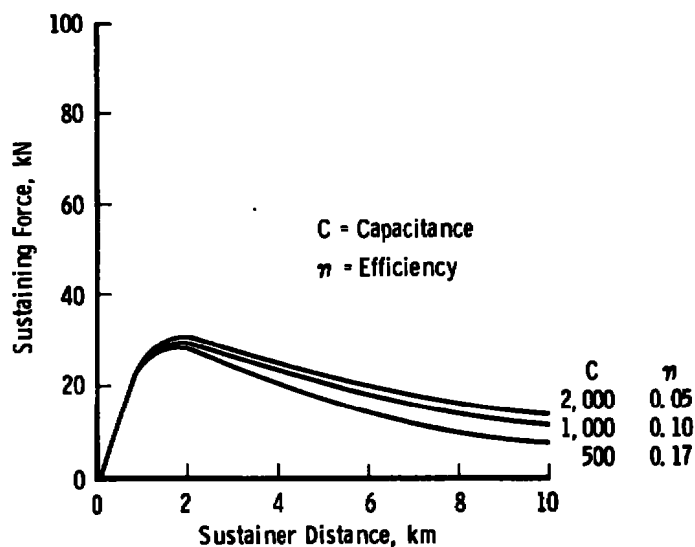


Figure 36. Force profiles for various capacitances.

To put the value of the sustaining force shown in context, if sustaining takes place over the entire range then the maximum force required to reach a β of 150 kN/m^2 ($3,000 \text{ lb/ft}^2$) is about $1,200 \text{ MJ/30 km} = 40 \text{ kN}$. Therefore, except for very long sustainers, an initial voltage of the order of 2 kV or less would be adequate.

If we now consider the worst case, that is, sustaining a 25- to 30-cm-diam model launched from a gas gun, we can derive the required stored energy as a function of range length and sustainer length using the results of Figs. 25, 28, and 35. The combined results are depicted in Fig. 37. For cases other than 25- to 30-cm-diam models sustained to a β of 140 kN/m^2 , the values on Fig. 37 may be reduced proportional to the total sustainer energy required as depicted in Fig. 25.

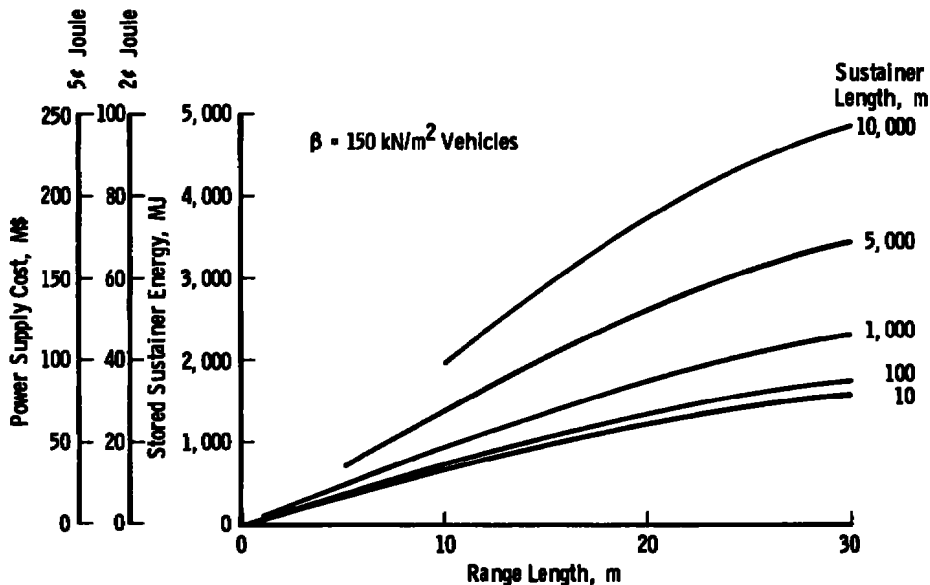


Figure 37. Stored energy versus range length.

3.2.4.3 Costing

To assist in evaluating the costs, the sustainer system will be divided into the power supply and the sustainer itself (rail gun) and treated separately.

1. Power Supply

The power supply consists of a capacitor (either an ordinary capacitor or a homopolar generator) and a small amount of "trimming" inductance of the order of 8 to 10 percent of the gun inductance. The inductance will be of comparatively low cost, so the power supply cost will be essentially that of a capacitor bank or homopolar generator capable of supplying the energies depicted in Fig. 37.

The energies involved are in the economical homopolar generator range (Ref. 13); however, the voltages required (1 to 2kV) are somewhat above present single machine capability. A number of series rotors and/or complete machines should be capable of reaching this voltage. Two cost scales are indicated on Fig. 37. Homopolar generator storage, above 500 MJ, should cost somewhere between two and five cents per joule, probably closer to two cents per joule.

2. Sustainer

The sustainer consists of the rails and the restraining structure necessary to hold the rails together and in alignment.

The rails are of copper and have a total volume of

$$\text{Vol} = 4hds_s = Dds_s$$

where h is the rail height ($= (1/4)D$), D the diameter, d the rail thickness, and s_s the sustainer length. To minimize the resistive losses d must be approximately equal to the electrical skin depth for the sustaining time, i. e. ,

$$d = \sqrt{\pi \zeta^2 t / u_0}$$

which for copper is $d = 0.22 t^{1/2}$. Now the transit time t is given by $t \approx s_s / v$, so the volume may be written as

$$\text{Vol} \approx 0.22 D s_s^{3/2} / v^{1/2}$$

and the mass as $m = 0.22 \rho D s_s^{3/2} / v^{1/2}$. Using a cost of ten dollars per kg for copper installed, the cost of the rails at $v = 5,000$ m/sec is

$$C_{R1} = 277 D s_s^{3/2} \$$$

Consider a restraining structure such as that depicted in Fig. 38. This is not suggested as a serious design, but only as an aid to calculating the approximate amount of material required.

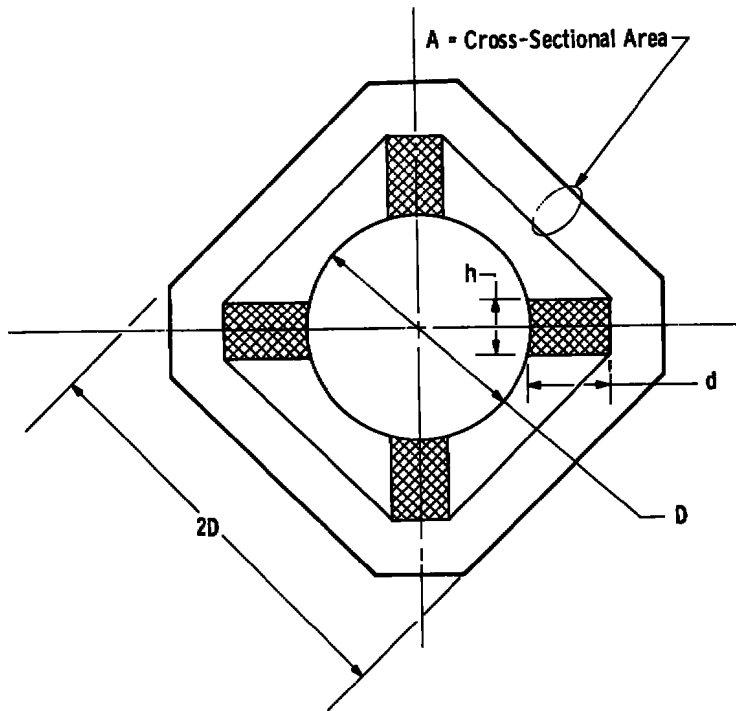


Figure 38. Possible restraining structure.

Each "member" of the restraining structure has a cross-sectional area A and absorbs approximately the entire load from one of the rails. If the bursting force on the rail is designated as F_R , then

$$F_R = L_R' (I/2)^2 / 2$$

where L_R' is the derivative of the inductance of the rails with respect to radial movement and only one-half the total current flows in one rail. I^2 can be related to the sustaining force by $I^2 = 2F_S/L'$, which reduces the above equation to

$$F_R = L_R' F_S / 4L'$$

L_R' can be evaluated from Fig. 3 and is found to be

$$L_R' \approx 0.4 \times 10^{-6} (s_s/D) H/m$$

Substituting this and $L' = 0.6 \mu\text{H/m}$ into the previous equation provides

$$F_R = 0.67 s_s F_s / D$$

The required cross-sectional area A is therefore

$$A = F_R / \sigma_s$$

where σ_s is the stress in the member. The volume of material in the restrainer structure is approximately $8DA$; therefore, the mass is

$$\begin{aligned} m &= 8\rho DA \\ &= 8\rho D F_R / \sigma_s \\ &= 5.36 \rho s_s F_s / \sigma_s \end{aligned}$$

If steel is used for the restraining structure, $\rho = 7.2 \times 10^3 \text{ kg/m}^3$, $\sigma = 2 \times 10^8 (\text{N/m}^2) (30,000 \text{ psi})$, $F_s = 40,000 \text{ N}$ (typical value), and the cost of steel installed is say ten dollars per kg, then the cost of the restraining structure is

$$C_{\text{Rst}} = 77 s_s \text{ \$}$$

The total cost of the sustainer itself is then the cost of the rail plus the cost of the restraining structure.

$$\text{Cost} = 77 s_s + 277 D s_q^{3/2}$$

and this is illustrated in Fig. 37.

The sustainer cost is predominantly that of the rails due to the large amount of copper required to minimize resistive losses. The rail cost could be lowered by reducing the thickness of the rails; however, this would increase resistive losses, lower efficiency, and require greater stored energy. Any saving would depend on the rate at which efficiency drops and on the relative costs of copper and energy.

3.2.5 Sustainer Example

As an example of a specific sustainer/range configuration that might be chosen, consider a range of 10-km length with five 1,000-m-long sustainer units and a 25-cm-diam projectile. From Fig. 37 the

power supplies would cost a total of about twenty thousand dollars (at two cents per joule for homopolar generator storage). The sustainers would cost about two thousand dollars each or a total of ten thousand dollars (Fig. 39). Therefore, the total cost of the sustainer system would be about thirty thousand dollars.

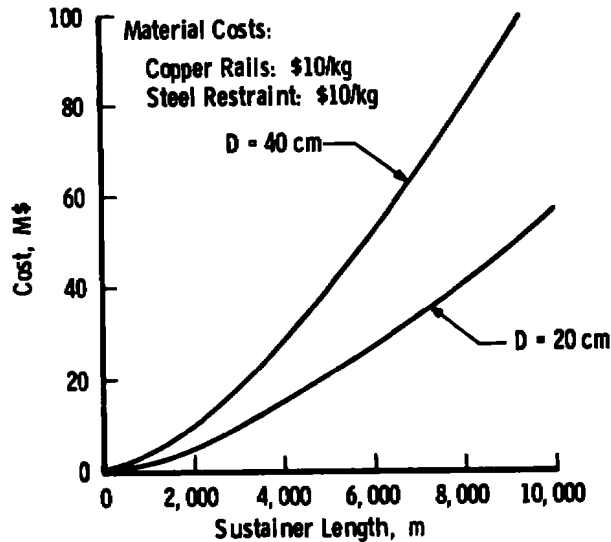


Figure 39. Cost per sustainer.

4.0 CONCLUSIONS

The purpose of this investigation has been to assess the technical and economic feasibility of employing the electromagnetic rail gun acceleration principle for the launching and/or velocity sustaining of large reentry test models. The limitations to rail gun performance that have been considered are ohmic heating of the projectile, electromagnetic instabilities, sliding contact behavior, and energy storage/rail gun driving methods. The following results and conclusions emerge from the study.

4.1 LAUNCHER

A rail gun capable of launching large diameter models up to 6 km/sec (20,000 ft/sec) appears to be technically feasible, except

for the unknown sliding contact behavior. Ohmic heating, electromagnetic instabilities, and driving method all impose constraints on the gun-projectile configuration, but these constraints are well outside the operational ranges of interest. A 200-m long (660 ft), inductively driven gun could launch projectiles of ballistic coefficient up to 150 km/m^2 to 6 km/sec.

Sliding contacts at the velocities envisioned here have not previously been studied, so it is difficult to assess the feasibility of operating sliding electrical contacts at the velocities and currents of interest here. However, work at the ANU, in which current densities are a factor of three higher but sliding distance is an order of magnitude lower, has shown that it is possible to obtain good electrical contact and acceptable mechanical sliding up to 1 km/sec. At this velocity, on the ANU rail gun, the contacts become unstable and arc. The effect on this instability of current density, projectile size, and projectile-rail materials has not been investigated so it is difficult to extrapolate to the ranges of interest here. The author's assessment of the contact problem is that there is no good evidence that contacts could not be made which would carry the required currents at the required velocities but then an appreciable development program would have to be undertaken.

The assessment of economic feasibility of a rail gun launcher is left to the reader. The cost of a launcher would be almost entirely that of the power supply as illustrated in Fig. 20. The rail gun is relatively inexpensive as shown in Fig. 17. A reasonable estimate of the cost for a power supply at these energies is about two cents per joule (1974). From Fig. 20, this yields a launcher cost of between \$60 million for a 20-cm gun to about \$180 million for a 40-cm gun.

4.2 SUSTAINER

A rail gun velocity sustainer also appears to be technically feasible except for the unknown sliding contact behavior. Ohmic heating, electromagnetic instabilities, and driving method would permit operation in the ranges of interest.

The same sliding contact difficulties arise in a sustainer as were noted in the launcher discussion, except that a sustainer would have much longer sliding distances, higher average velocities, and considerably lower currents. These factors would be expected to make the sustainer contacts behavior more mechanically dominated than the launcher

contacts. However, the lack of knowledge of high-speed contact mechanical behavior would require a similar development program to that envisioned for a launcher to be undertaken.

Estimated costs for a sustainer power supply and rail structure are shown in Figs. 37 and 39. Again, a good figure for energy costs is about two cents per joule. A range length, sustainer length, and sustainer number must be chosen to arrive at a complete cost. Typically, a 10-km range with five 1,000-m sustainers would cost about \$30 million. The assessment of economic feasibility is left for the reader.

In conclusion, both rail gun launching and velocity sustaining of large reentry models appear to be technically feasible, except for the little understood behavior of high-speed sliding contacts. An experimental development program on sliding contacts would have to be undertaken to finally establish feasibility.

REFERENCES

1. Millsaps, K. and Pohlhausen K. "The Linear Acceleration of Large Masses by Electrical Means." AFMDC-TR-60-11, Holloman Air Force Base, New Mexico, 1960.
2. Chapman, R. L., Harms, D. E., and Sorenson, G. P. "The Magnetodynamic Hypervelocity Gun." Sixth Symposium on Hypervelocity Impact, Vol. 1, 1963, pp. 319-330.
3. Braste, D. E. and Sawle, D. R. "Feasibility Study for Development of a Hypervelocity Gun." NASA-CR-60119, 1964.
4. Sawle, D. R. "Hypervelocity Impact in Thin Sheets and Semi-Infinite Targets at 15 km/sec." AIAA Journal, Vol. 8, No. 7, July 1970, pp. 1240-1244.
5. Barber, J. P. "Experimental Observations on Rail Gun Acceleration." ARA Proceedings, AEDC, Tullahoma, Tennessee, 1973.
6. Grover, F. W. Inductance Calculations, Working Formulas and Tables. Dover Publications, New York, 1962.
7. Cnare, E. C. "Magnetic Flux Compression by Magnetically Imploded Metallic Foils." Journal of Applied Physics, Vol. 37, 1966, pp. 3812-3816.

8. Bowden, F. P. and Tabor, D. "The Friction and Lubrication of Solids." Clarendon Press, Oxford, 1953.
9. Graff, K.F. and Detlaff, B.B. "The Gouging Phenomena Between Metal Surfaces at Very High Sliding Speeds." Wear 14, 1969, pp. 87-97.
10. Holm, R. "Electric Contacts." Springer Verlag.
11. Bowden, F. P. and Williamson, J. B. P. "Electrical Conduction in Solids I. Influence of the Passage of Current on the Contact Between Solids." Proceedings of Royal Society of London, Series A, Vol. 246, 1958, pp. 1-13.
12. Barber, J. P. "The Acceleration of Macroparticles and a Hypervelocity Electromagnetic Accelerator." EP-T12, Department of Engineering Physics, Australian National University, Canberra, Australia, 1972.
13. Lukasiewicz, J. et al. "Development of Capacitance and Inductance Driven Hotshot Tunnels." AEDC-TN-60-222 (AD249421), January 1961.

NOMENCLATURE

A	Cross-sectional area
a	Acceleration
A_b	Actual metal-to-metal contact area
A_r	Reference area
A_{bn}	Area of solid-to-solid contact at point n
a_D	Desired drag deceleration
a_s	Sustainer acceleration required
B	Magnetic flux density
b	Thickness of rails
C	Capacitance
C_D	Drag coefficient
C_{gun}	Cost of gun
Cost	Total cost of sustainer
C_{Rl}	Rail cost
C_{RST}	Cost of restraining structure
D	Model diameter
d	Projectile thickness
E	Energy
E_d	Drag energy
E_s	Energy required for sustaining
E_{store}	Stored energy required
e	Density of test environment
F	Force
F_d	Retarding forces of friction and drag
F_f	Frictional force
F_R	Bursting force on rail
F_s	Sustaining force required
F_{sn}	Sustaining force provided by n^{th} segment of sustainer
g_1	Ohmic heating action constant

h	Height of rails
I	Electric current
i	Electrical current density
I_0	Initial current
K_{rail}	Cost of rail per unit volume
K_{restrain}	Cost of restraint per unit volume
L	Inductance
L'	Inductance per unit length
L'_R	Derivative of rail inductance with respect to radial motion
L_0	Fixed inductance
l	Flight path length
m	Mass
n	Number
P	Normal load on contact surface
P_m	Magnetic pressure
Q_m	Specific energy required to melt material
R	Electrical resistance
R'	Resistance per unit length
r	Radius
R_0	Fixed resistance
S	Tangential force required to shear points of contact
s	Shear strength of material
s_s	Sustainer length
t	Time
t_{rail}	Rail thickness
V	Voltage
V_0	Initial voltage
V_{rail}	Volume of rail material

V_{restrain}	Volume of restraining material required
v	Velocity
\bar{v}	Average velocity
v_f	Final test velocity
v_{max}	Maximum launch velocity as $L_0 \rightarrow \infty$
v_0	Initial velocity
v_r	Relative velocity, v/v_{max}
W	Power
w	Width between rails
x	Distance along rail from breech
x_L	Accelerator length
α	Ratio of L' to L'_0
β	Ballistic coefficient
β_0	Designed ballistic coefficient
γ	Acceleration ratio, $a_{\text{average}}/a_{\text{maximum}}$
γ_s	Fraction of flight path which is provided with sustainer
δ	Electrical skin depth
δ_w	Wear depth per unit area
ζ	Electrical resistivity
η	Energy efficiency of acceleration
μ_f	Coefficient of friction
μ_0	Magnetic permeability of free space
σ	Average yield stress
σ_s	Stress
ϕ	Magnetic flux
ϕ'	Magnetic flux per unit length